WCD-2021-18

Identification, characteristics, and dynamics of Arctic extreme seasons

Response to the Reviewers' comments by Katharina Hartmuth, Maxi Boettcher, Heini Wernli, and Lukas Papritz

We thank the editor and all three reviewers for their insightful and helpful comments. We address each comment point by point below. The editor's and reviewers' comments are given in blue and our responses in black. The most important aspects of our replies and revisions are:

1) As suggested by reviewer 1, we used the North et al. approach to show that the first two PCs are statistically distinguishable from the others.
2) We now better explain the several subjective choices that were necessary for our analyses.
3) We clarify our choice to use a multivariate approach to explore different types of extreme seasons.

Please note, that we always refer to the lines in the **revised manuscript** (document without track changes). Figures in the reply document are referred to as "Fig. R1", etc., and figures in the revised manuscript are referred to as "Fig. 1", etc. We further supplement this document with a pdf containing track changes (latexdiff-pdf showing changes from first manuscript version to revised manuscript).

Editor

All three reviewers appreciated the study, and I agree with them that the work represents an interesting and important contribution. Some valid concerns are raised in their thorough and insightful reviews, and the authors have provided good indications of how they will address these concerns. In preparing a revised manuscript, I would encourage the authors to focus particularly on a few points which many of the reviewers' comments group around. Also, there remain small English usage errors throughout (some but not all mentioned by the reviewers).

1) Interpretation of identified extreme seasons, mentioned in detail by R2 and also touched on by R1 (anomalous vs extreme) and R3 (rescaling). I believe it would be worth spending some more time to put results from this method in context of results from conventional approaches (R2 comment #1), which would also go towards highlighting the impact/novelty of this study.

Thank you for this comment. We extended the discussion of our method and did our best to better highlight the novelty and differences of our approach compared to a more conventional method (such as, e.g., simply choosing the warmest or wettest seasons).

We further updated Table 2, which now includes the rank for each seasonal-mean anomaly (with respect to all seasons) of our identified extreme seasons. We can show that each extreme season has an extraordinary seasonal-mean anomaly (rank 1 or 2) for at least one parameter.

Thus, the extreme seasons identified with our method would also be identified with a more classical approach (e.g., the extreme summers 2013 and 2016, which show the most negative and most positive $\overline{T_{2m}}^{*}$, respectively, in the whole study period). However, with our method we also identify anomalous seasons that are characterized by an unusual combination of seasonal mean anomalies, each of which is not particularly noteworthy (in terms of their rank). We have included a discussion of the benefits of our approach over a more classical one in the discussion (Section 6).

For further details see responses to reviewer questions (R1: general comment (1) and specific comments (2,15), R2: general comment (1) and R3: specific comment (8)).

2) Clarification of methodology (all reviewers), including the choice of winter case studies only.

We included all suggestions from the reviewers to clarify and improve the discussion of our method throughout the manuscript. At the end of chapter 4 (L363ff.), we included a more detailed justification for the choice of our three case studies.

3) Sharpening of the presentation (e.g., many nice suggestions from R2, R3 regarding framing questions). I agree with the authors that the length is fine, especially given the amount of work that has been done, but the text could be edited to better guide the reader to the main messages. It could help also in the abstract and conclusions to put more weight on what we learn about point #1 and less weight on details of the case studies.

Thank you for these remarks. We added some metadiscourse at the beginning/end of a few sections to ensure a better guidance of the reader. We further sharpened our main messages by integrating the reviewers' suggestions and, e.g., adding further discussion of our method in the discussion chapter (L584ff.).

Reviewer 1

General comments

The authors evaluate the atmospheric conditions during anomalously extreme seasons in the Arctic. This is performed using a regional principal component (PC) analysis (PCA) from ERA5 data of the first two PCs of all seasons from 1979-2018. Furthermore, the PCA uses six key surface variables and divided spatially into 9 Arctic sub-regions. The sub-regions are subjectively chosen, but based on climatological sea ice conditions in either the Nordic Seas, Kara-Barents Seas, and the rest of the Arctic. Results identify 2-3 extreme seasons for each season (DJF, MAM, JJA, SON) in each sub-region. The PCA applied here provides a quantification of which variables contribute most to the extreme conditions of the respective season, and how consistent those conditions are during those particular seasons. The authors then choose two extreme seasons in the Kara-Barents sea during winter (DJF) to further investigate the synoptic weather conditions that were occurring and how they might have lead

up to the resulting seasonal extremes. The chosen seasons are picked based on their orthogonal, yet extreme, projections onto the PCs.

This research nicely demonstrates how PCs can be used to identify seasonal anomalies and extremes in certain regions of the Arctic. It furthermore demonstrates how to use that information to provide an expectation of how an extreme season was characterized with regard to one of the six variables and how consistent those conditions were. It is certainly a nice way to be able to identify extreme seasons that might be worth analyzing in further detail at shorter time and space scales if desired. Overall, I think these results can make a contribution and be published once some remaining issues are addressed. In particular:

1) Picking the first two principal components is subjective and does not necessarily isolate most of the variance. It first needs to be established that the first two principal components are the only significant ones. I do not doubt that this is the case given that on line 282, it is stated that they usually explain 80-90% of the variance. However, it should be shown that they are indeed statistically distinguishable from the others. North et al. (1982) provide a well-established method of statistically distinguishing the first few eigenvalues from the others.

Thank you for this comment and for pointing us to the method introduced by North et al. We applied this method and the results reveal that the first two PCs in DJF and JJA are, with the exception of sub-region **ARM** in JJA, always statistically distinguishable from the others. We added this information to the revised manuscript (L305ff.). Here we provide further details about our results from applying the North et al. (1982) method, which we also show in the supplement.

Figures R1 and R2 show the standard errors for each eigenvalue in our PCA as introduced by North et al. (1982) for each sub-region in DJF (left-hand side) and JJA (right-hand side), respectively. The estimate for the standard error is given by

$$\delta\lambda_{\alpha} \approx \lambda_{\alpha}(2/N)^{1/2},$$

where λ_{α} denotes the respective eigenvalue and N the sample size, which in our case corresponds to the 39 realizations of the four seasons of the study period. Along the y-axis, the eigenvalue for each Principal Component (PC) is given and the error bars represent the estimated standard error. For both seasons, the first two eigenvalues, λ_1 and λ_2, are either clearly distinguishable or their error bars show only a very small overlap, except for sub-regions **KBI** and **NOM** in winter. Further, λ_1 and λ_2 are always clearly distinguishable from the third eigenvalue λ_3. The only exception is the sub-region **ARM** in JJA for which the error bars of λ_2 and λ_3 have a significant overlap. Thus, we can show that the first two PCs, which we use for the definition of our extreme seasons and which explain between 80%-90% of the variance in the respective sub-regions, are almost always statistically distinguishable from the remaining eigenvalues. We conclude that PC1 and PC2 isolate most of the variance and the corresponding eigenvalues are statistically distinct.

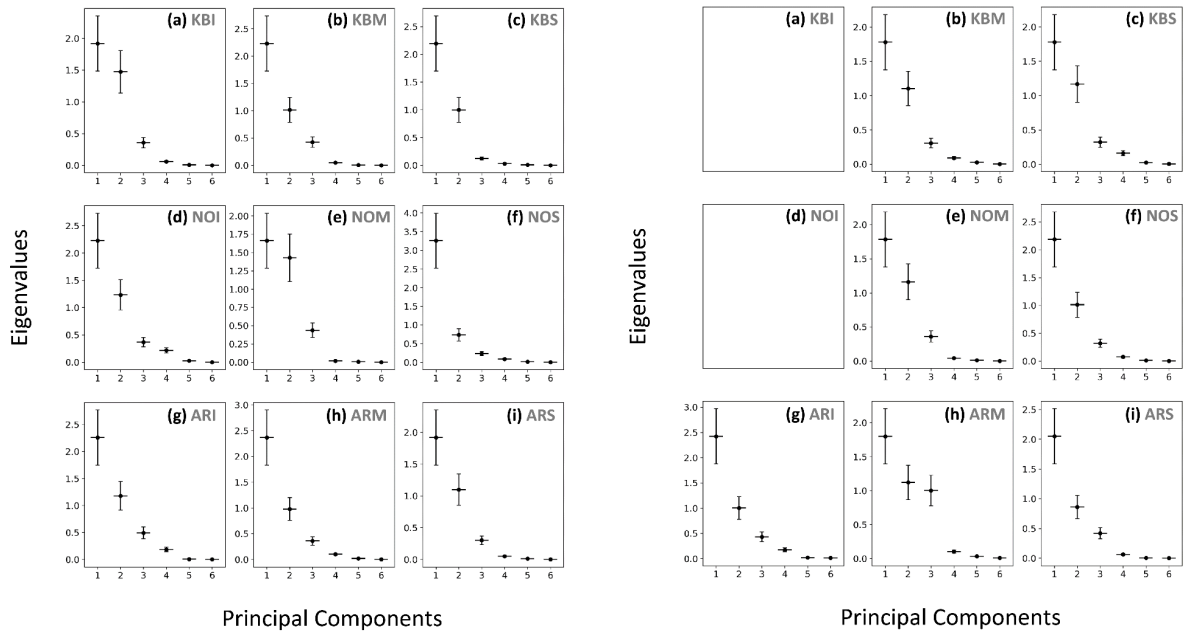

Figures R1 and R2: Standard errors for each PCA eigenvalue for all sub-regions in DJF (Fig. R1) and JJA (Fig. R2). The number of the Principal Component is given along the x-axis and the eigenvalue of each Principal Component along the y-axis. Error bars denote the estimated standard error following North et al. (1982).

2) Section 3 and generally throughout: The values of all correlations and their p-values that are described should be listed in a table.

We agree that it would be helpful to add a list containing all correlations and respective p-values for the described relations between the different parameters. We thus added such a table to the supplementary material and refer to it in the paper.

3) Figures 5 and 6 are a very nice way to illustrate the seasonal anomalies and the variability that may have also been occurring within those seasons. Having never seen these diagrams before, it at first takes a little bit of time to understand. It would be very helpful if there were a schematic showing the "phase space" of the interpretation that illustrates what is said in words on lines 251-258 (i.e., regions on the graph where there would be anomalies that tend to be continuous, where there would be warm episodes alternating with weak cold episodes, where there would be several intense warm and cold episodes that nearly cancel, where they would be near the climatology, etc.).

Thank you very much for pointing this out. To better understand and interpret the figures, we added lines of a constant ratio of the seasonal-mean anomaly and the seasonal-mean absolute anomaly ($\frac{\overline{\chi^*}}{|\overline{\chi^*}|}$) to the diagrams, such as you can see in the schematic figure below. We further adapt lines 258-278 in the revised manuscript as follows:

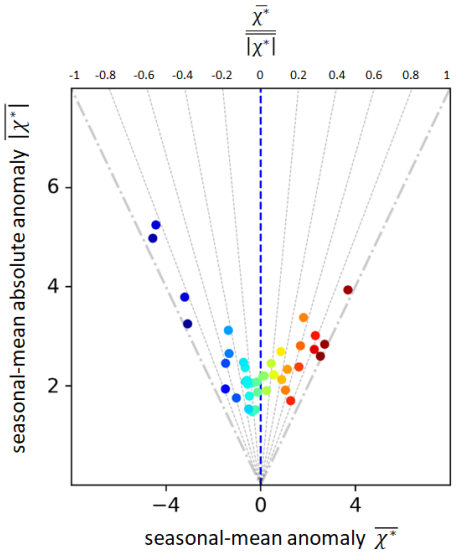

Figure R3: Schematic figure showing seasonal-mean anomalies ($\overline{\chi^*}$, along x-axis) vs. seasonal-mean absolute anomalies ($|\overline{\chi^*}|$, along y-axis). The dots in this schematic figure are colored by the ratio of both measures, $\frac{\overline{\chi^*}}{|\overline{\chi^*}|}$, which is additionally visualized by grey dashed lines. $\frac{\overline{\chi^*}}{|\overline{\chi^*}|} = \pm 1$ is shown by stippled grey lines and $\frac{\overline{\chi^*}}{|\overline{\chi^*}|} = 0$ is shown by a dashed blue line.

'To better understand the seasonal substructure of Arctic winters and summers, we compare the seasonal-mean anomalies ($\overline{\chi^*}$) with the seasonal-mean absolute anomalies ($|\overline{\chi^*}|$) for T_{2m}, P and E_S in selected sub-regions in DJF (Fig. 5) and JJA (Fig. 6). The ratio of seasonal-mean and seasonal-mean absolute anomalies, $\frac{\overline{\chi^*}}{|\overline{\chi^*}|}$, is indicative of the temporal persistence of an anomaly throughout a season. Thus, the location of a season in the diagrams provides information about the substructure of the season in terms of the considered parameter. In general, the further to the right, the more positive is the seasonal-mean anomaly of the shown parameter and the further to the left, the more negative. The closer the seasonal-mean anomaly is to the seasonal-mean absolute anomaly (dots close to the outer stippled grey line representing $\frac{\overline{\chi^*}}{|\overline{\chi^*}|} = \pm 1$), the more persistent the anomaly is throughout the season. Thus, we define seasons with $0.8 \leq \frac{\overline{\chi^*}}{|\overline{\chi^*}|} \leq 1$as seasons with a "continuous" anomaly. With a decreasing absolute value of$\frac{\overline{\chi^*}}{|\overline{\chi^*}|}$, the seasons are located further away from the outer stippled grey lines, meaning that positive or negative anomalies in the respective parameter occur more episodically throughout the season. The closer a season is positioned towards the blue dashed line where $\overline{\chi^*} = 0$ and thus $\frac{\overline{\chi^*}}{|\overline{\chi^*}|} = 0$, the more positive and negative daily anomalies cancel each other, leading to a weak overall seasonal anomaly. The value of $|\overline{\chi^*}|$ is further indicative of the magnitude of the daily anomalies throughout a season. A season located at the top of the plot shows stronger daily anomalies than a season with the same $\frac{\overline{\chi^*}}{|\overline{\chi^*}|}$ratio but a smaller $|\overline{\chi^*}|$.

For example, a season can be anomalously warm because the daily-mean T_{2m} values are larger than the climatology on almost all days of the season , resulting in $\frac{\overline{T_{2m}^*}}{|\overline{T_{2m}^*}|} \approx 1$. With a decreasing ratio of both anomaly metrics, e.g.$\frac{\overline{T_{2m}^*}}{|\overline{T_{2m}^*}|} = 0.5$, the season is still anomalously warm, but it

results from several warm episodes alternating with weaker and/or shorter periods with negative T_{2m}* values. If $\frac{\overline{T_{2m}^{*}}}{\overline{|T_{2m}^{*}|}} \approx 0$, cold and warm episodes cancel each other leading to a weak overall seasonal anomaly. Comparing two seasons with the same $\frac{\overline{T_{2m}^{*}}}{\overline{|T_{2m}^{*}|}}$, the season which is positioned further up in the plot (showing larger values of $\overline{|T_{2m}^{*}|}$ and $\overline{T_{2m}^{*}}$) shows a larger variability in T_{2m} with more intense warm and/or cold episodes compared to the season which is located further down.'

4) The justification for choosing two winter cases is weak. Perhaps this is because the anomaly values are smaller in the summer. But is it not dM and the standardized anomalies that determine how extreme a season is with these methods? These are just as strong in the summer (Table 2). I can see that the results shown in Figure 5 are used to pick the cases, but again, this seems contrary to the main setup of this paper of using the PCs to determine the extremes. Also, why 2011/12 in the Kara Barents Sea when this categorizes as "anomalous" rather than "extreme" in these methods? Regardless, it is hard to justify the title "Identification, characteristics, and dynamics of Arctic extreme seasons" when only the dynamics of winter extreme seasons were discussed.

We agree that our choice of the case study seasons (three winter seasons, two in the Kara and Barents Seas, and one in the High Arctic) is subjective. They are also to a certain extent a compromise between “many more seasons would be interesting to study in greater detail” and “the paper should remain readable and have a reasonable length”. We think that choosing three winter seasons makes their comparison easier and their differences more revealing. We would like to show that even in the same region (Kara and Barents Seas) two anomalous/extreme winter seasons can have a completely different substructure and can be associated with different weather systems, emphasizing the inter-annual variability. Showing this for a winter and a summer season would be less surprising and interesting as this would mix seasonal and inter-annual variations. It is also important to us to evaluate the case studies in some depth, which limits the number of cases fitting into the paper to about three. Of course, we also looked at other seasons but then decided that the selected cases nicely illustrate the diversity and complexity of the involved processes, which is one of the key aims of our study. In the revised version we now better explain that the choice of the case studies is subjective and motivated by our intention to reveal the diversity and complexity of the involved processes (L363ff.).

Regarding the title, it’s true that we identify and characterize extreme seasons in summer and winter, but then only discuss the dynamics in winter. However, as we now explicitly mention this limitation and better explain the key aim of the case studies, we think that the title is justified.

Specific comments:

1) Line 135: Why are only marine cold air outbreaks (CAOs) considered? There are also significant CAOs over land, described in Biernat et al. (2021).

We are only considering ocean and ice grid points and thus only marine cold air outbreaks, which are identified on grid points with less than 50% sea ice.

2) Line 186: Choosing a dM threshold of 3 seems quite subjective. How is this threshold picked? If each principal component has a significant anomaly of two standard deviations, this could provide an expectation for what would be significant when considering the PCs in combination.

The thresholds for anomalous resp. extreme seasons are indeed a rather subjective choice. However we find that with these thresholds we obtain on average 0-1 extreme seasons per sub-region (which equals 0-2.5% of all seasons) and 4-5 anomalous seasons per sub-region (equalling 15-17% of all seasons). Assuming a normal distribution, these values correspond to the range of 2-3σ for our extreme seasons and 1-2σ for our anomalous seasons. Further, with this number of extreme seasons, the return period of such a season corresponds to approximately 40 years. Several studies, e.g., Röthlisberger et al. (2021) used this as an adequate measure for defining extreme seasons.

As a side note, we would like to mention that preliminary analyses of 1000 years of (present-day) CESM large-ensemble data show that our chosen threshold of d_M=3 results on average in a return period of around 70-90 years. We are, thus, confident that classifying the seasons with d_M>3 as “extreme” is well justified.

3) Line 219: Be more specific about "almost always." What percentage of the time is it true? Same thing for line 225... what percentage of the cases translates to `usually'?

Thank you for pointing this out. We adjusted the manuscript in the indicated section (L225ff.) to clarify the mentioned relationships between the different variables.

4) Line 262: How close to the |P*| = P* line does a season need to be in order to be called "continuous?" For example, the 2016/2017 winter season was pretty close, but not exactly on it. On the other hand, there are very few cases of |T2m*| = T2m* being exactly equal in the summer while it is described as "continuous" on line 260.

There are indeed only very few cases where the seasonal-mean and seasonal-mean absolute anomalies of a season are equal. Thus we changed our definition of a “continuous anomalous season” from $\overline{|\chi^*|} = \overline{\chi^*}$ to $\overline{|\chi^*|} \approx \overline{\chi^*}$, including seasons with a ratio of $0.8 \leq \frac{\overline{\chi^*}}{\overline{|\chi^*|}} \leq 1$(see previous comment). We added these changes to the revised manuscript (L265ff.).

5) Line 307: Would also be useful to point out that there is very little 2-m temperature variability over the Arctic sea ice in the summer. This could imply that temperature variability may not play a major role in sea ice loss, which has very large interannual variability in the summer.

Figure 8 does indeed suggest that T_{2m} has only little variability in regions with SIC_{clim}>0.9 in summer compared to other sub-regions. However, T_{2m} is capped above sea ice as the air is cold and the excess energy goes into the melting of the ice if T_{2m} is above the freezing point, which essentially limits (near-surface) temperature variability. We further assume that the sea ice loss in summer is equally strong in the other sub-regions (especially the mixed sub-regions with very variable SIC), which show a larger variability in SIC. As there exists only one sub-region with SIC_{clim}>0.9 in summer, we think that additional analyses would be needed to make such a statement.

6) The justification of how an extreme season is chosen on Lines 310-314 should be moved up to Section 2.3.

We already explain this in Sect. 2.3. The text in lines 334ff in the revised manuscript is meant as a reminder. We now clarify this by writing “As explained in Sect. 2.3, …”.

7) Line 315: Which season does Figure 2 show? This could also be referenced here along with Table 2.

Figure 2 in the manuscript is only a schematic biplot which does not refer to a specific season nor region. We slightly changed the figure caption to clarify that this is only an idealised plot.

8) Figures 9, 10, 14: Would be helpful to label the x-axis with the month/date instead of the day of the season, esp. to be consistent with the text.

We mostly use “on day 12,15, 20…” throughout the text and only rarely real dates. Thus, we adapted the manuscript such that we don’t use specific dates anymore, as we think that this ensures better readability.

9) Line 367: How are blocking, cyclone, and CAO frequencies computed exactly? Need references and a short description.

A common feature of our weather system identification schemes is that they produce a two-dimensional binary field, often referred to as the “mask” of the weather systems, where grid points that belong to a system have a value of 1 and the others have a value of 0. Simple time averaging of these binary fields then automatically delivers the weather system frequency field. For example, if a cyclone mask covers a grid point at 25% of all times, then averaging 25% times a value of 1 and 75% a value of 0 leads to a frequency of 0.25 (we added this information in lines 397ff.). For the specifics of the identification scheme, we added a few sentences for each weather system and now give the relevant references to the papers that introduced these schemes in lines 132ff.

10) Line 389: "Several episodic precipitation events..." But wouldn't Fig. 5h suggest consistent precipitation events?

Thank you for pointing this out. We deleted “episodic” to clarify the constant occurrence of precipitation events throughout the season.

11) Line 431: Remove "it is obvious that"

We changed “it is obvious that” to “it can be seen that”.

12) Line 440: Please also label JJA 2016 in Figs. 6 and 8.

To make it clear that JJA 2016 is somehow connected to our case study DJF 2016/17, we additionally labeled it in Figs. 6 and 8 in the manuscript.

13) Lines 441-445: It is misleading to say that there were positive temperature anomalies over large parts of the Arctic in JJA 2016. This and the blocking was more centered over the Kara-Barents Sea region, while much of the central Arctic was not exceptionally warm and had frequent cyclones.

We are not sure if we understood your remark correctly, as we do not state that the positive surface temperature anomalies in JJA 2016 occurred over large parts of the Arctic, but only in the Kara and Barents Seas. We then state that in autumn 2016 (mainly during October and November), positive temperature anomalies occurred across the whole Arctic region as already shown by Tyrlis et al. (2019). We now clarify this further in the text by replacing “during autumn 2016” by “during October and November 2016” (L482).

14) Section 5.3: If the blocking frequency was greatest over Scandinavia, why were the warmest temperature anomalies over the Kara-Barents (KB) region and not co-located with the blocking? Seems like there should have been northerly flow over much of the KB region from air flowing over sea ice. Is it surprising that the air mass was not modified by the time it reached KB?

Thank you for pointing this out. First of all we want to emphasize that DJF 2016/17 was not a particularly warm season, but experienced several episodic warm events. Blocking over Scandinavia influenced the surface temperatures in the Kara and Barents Seas, especially during the warm episode in February 2017. Trajectories show that a majority of the air causing this warm episode originated over Scandinavia and was undergoing subsidence (we will add a short evaluation of some air mass trajectories to the supplement; see answer to comment (15) of reviewer 2 and Fig. R6). However, the pattern of blocking and cyclone anomaly patterns as shown in Fig. 12 in the manuscript does also support northerly flow into the region as you correctly assume, causing for example the period with a strong CAO in mid-February 2017, when cold air is transported from the High Arctic towards the South, facilitated by a block over Scandinavia and a cyclone in the eastern part of the Kara and Barents Seas. Please have a look at the supplementary animation S2 where we show the synoptic evolution for each day throughout the season. We also tried to further shape section 5.3 to better highlight in which way the synoptic patterns influenced the surface temperatures in our case study sub-regions.

15) Lines 120, 541: Is this approach really novel given that (Graf et al. 2017) first introduced it in a similar application?

Using a PCA for finding dominant variability modes has been done in several studies such as, e.g., Graf et al. (2017). However it has never been used to define anomalous or extreme

seasons based on the combination of several parameters. Thus, in terms of defining extreme seasons, this approach is novel. However, we deleted the word “novel” in L584 to clarify that the use of a multivariate approach per se is not novel.

Technical corrections:

1) Table 1: 2 m temperature --> 2-m temperature

We followed the WCD submission guidelines (see “House standards” for hyphen usage: “It is our house standard not to hyphenate modifiers containing abbreviated units (e.g. “3-m stick” should be “3 m stick”)).

2) Table S1: Caption states standardized values are in brackets, but they are instead in parentheses.

Thank you for spotting this. We replaced “brackets” with “parentheses” in the caption of Tables 2 and S3-S6.

3) Section 2 should be "Data and methods" given that there is more than one method used to complete the analysis.

Changed as suggested.

4) Figure 1 caption: State what the green and red boxes denote.

We added the following sentence to the caption of Figure 1: “Green and red boxes denote the areas of the Kara and Barents Seas and Nordic Seas regions, respectively.”

5) Line 135: There does not need to be a space between the number and the "%" symbol

Again, we followed the WCD submission guidelines (see Figure content guidelines: “Spaces must be included between number and unit (e.g. 1 %, 1 m).”).

6) Lines 140-141: What is the sign convention for the surface energy balance?

Thanks for hinting at this. We added the following sentence in L144ff.: “Positive signs denote energy fluxes into the surface, whereas negative signs are indicative for energy fluxes into the atmosphere.”

7) Line 183: There should be a period at the end of the equation.

A period has been added at the end of the equation.

8) Lines 352, 465: normal --> average

Changed as suggested.

9) Line 393: This --> These

Thanks for spotting this, we changed “this” to “these”.

10) Line 424: Remove "of"

“Despite of this” has been changed to “despite this”.

11) Line 453: Insert "of" after "Comparison"

“Comparison DJF 2011/12 and DJF 2016/17” → “Comparison of DJF 2011/12 and DJF 2016/17”.

12) Line 463: got --> became

Changed as suggested.

References:

Biernat, K. A., L. F. Bosart, and D. Keyser, 2021: A climatological analysis of the linkages between tropopause polar vortices, cold pools, and cold air outbreaks over the central and eastern United States. Mon. Wea. Rev., 149 (1), 189-206.

Graf, M. A., H.Wernli, and M. Sprenger, 2017: Objective classification of extratropical cyclogenesis. Quart. J. Roy. Meteor. Soc., 143 (703), 1047-1061.

North, G. R., T. L. Bell, R. F. Cahalan, and F. J. Moeng, 1982: Sampling errors in the estimation of empirical orthogonal functions. Mon. Wea. Rev., 110 (7), 699-706.

Reviewer 2

The paper presents an analysis of variability in three Arctic regions using 6 metrics. An input of those metrics into the dominant modes of variability and links between those metric are discussed. Overall, I am impressed by the amount and quality of work done in this study.

Here is what I like about the paper:

- Fig 5 and 6, which show that while strong anomalies may be observed in one or two metrics, other metrics may remain close to their climatological values;
- assessment of the input of the six metrics into the main modes of variability and relationships between them;
- case studies (particularly fig. 10,11, 14) and the discussion around them. An attempt to establish a connection between the weather and seasonal anomalies is valuable;

- a wide range of metrics used in the study - not only T2m/SIC/P, but also energy fluxes, cyclone frequency, CAO and a blocking index.

However, there is a couple of major concerns that need to be addressed before the paper can be accepted for publication:

1. I am not convinced that the approach, introduced in the paper, is a good way to select extreme seasons. Despite the use of a multivariate approach, it often comes to just one metric showing a strong seasonal anomaly, which was enough to identify the season as extreme or anomalous. Thus, without applying this approach, one may simply go through all 6 metrics and select the most extreme season(s) in each of them. I don't think I saw a proof that the seasons selected with the PCA analysis were more anomalous than those that showed a strong anomaly but were not picked up by the PCA approach. The latter may be even more anomalous than those, that were selected using the PCA.

On the other hand, there are seasons that were identified as anomalous though none of the variables showed a strong anomaly. Could it be proved that they are 'true' anomalous seasons and not artefacts of the method?

I am not asking for a change of the approach here, but I think more discussion around potential (dis)advantages of the proposed method is needed. In my opinion, this method identifies the dominant modes of variability and allows for assessment of the contribution of each of 6 metrics into those modes and a link between them. Section 5 explores a few seasons when one of the first two modes of variability was among the strongest.

We appreciate and fully understand this remark. It is a priori not clear how extreme seasons should be defined. An obvious choice, which we also use in other studies, is to simply choose the warmest or wettest seasons. This would prioritize one parameter (e.g. temperature or precipitation) and a justification would be given why this parameter is particularly relevant. Here we tried something else, something more "objective" in the sense that we did not want to pre-specify the most relevant parameter. Instead, we allow for the possibility that besides individual parameters, also their combination can be unusual. Thus, we were led by the hypothesis that our multivariate approach will lead to different types of extreme seasons (different in terms of their individual anomalies of T_{2m}, P and E_S), which, however, share a similar "anomalousness" as expressed by the parameter d_M. We don't think that this method produces artefacts; in order to reach a value of $d_M \geq 2$ (or even $d_M \geq 3$), at least one of the considered variables or a combination thereof must be clearly exceptional compared to the other seasons in the ERA5 time period. In the revised version we will make sure that this line of thought becomes obvious to the reader. At the same time, we cannot (and don't want to) prove that this approach is "better" than a more conventional one. If all that matters in a specific study is for instance the seasonal snow accumulation, then there is no need to work with our approach.

We adapted the discussion (L584ff.) to clarify the novelty and characteristics of our approach in the context of other, more conventional, methods.

2. My other concern is the length of the manuscript. Considering the amount of work, it is hard to make it shorter, but I think the paper will benefit from it. Some plots (especially, Fig. 3) are too busy and are difficult to interpret. Section 3 and 4, while interesting, are hard to read, particularly when plots discussed in the text are a couple of pages away (which is inevitable). Please select the most robust and/or important relationships and focus on them. I understand that each plot provides a lot of information, but, unfortunately, human beings can only keep a few facts in mind at a time.

We did our best to further streamline the text and make it as readable as possible. With regard to the length of the paper, we think that it is still fairly OK.

Other comments:

1) Abstract: 1.The abstract is a bit long, even if there is no word limit, a page-long abstract is not ideal.

Thank you, we shortened the abstract by about 20%.

2) I think it is worth mentioning that 2016/17 winter was mostly anomalous in terms of precipitation and maybe in some other variables, otherwise, until you read the paper, it remains unclear why it was anomalous.

Thank you for this remark. In the revised version of the abstract we write “In contrast, winter 2016/17 started with a strongly reduced sea ice coverage and enhanced sea surface temperatures in the Kara and Barents Seas. This preconditioning, together with increased frequencies of cold air outbreaks and cyclones, was responsible for the large upward surface heat flux anomalies and strongly increased precipitation during this extreme season.” This makes it clear that DJF 2016/17 was mainly anomalous in terms of precipitation and surface heat fluxes.

3) Sect. 2.3: For the PCA analysis, was each metric first averaged over the corresponding region? Meaning that the special structure of those anomalies was not accounted for.

Yes, we average over the region and therefore lose information about the spatial structure.

4) Fig. 3: As I already mentioned above, it is a very busy plot, which is hard to read. The only thing that is obvious to me is that in JJA the red/blue markers can be linked to positive/negative temperature anomalies. For DJF, what is obvious is a link between T2m and P anomalies and that the low right corner has predominantly negative Es anomalies. However, regional differences, discussed in the text, are very hard to see. If you decide to keep this plot, maybe splitting into different geographical locations or the sea ice concentrations helps.

Thank you very much for the suggestion. We adapted the figure (Fig. R4 below shows the revised Fig. 3 of the paper), and now show the correlations for each SIC_{clim} range in separate panels.

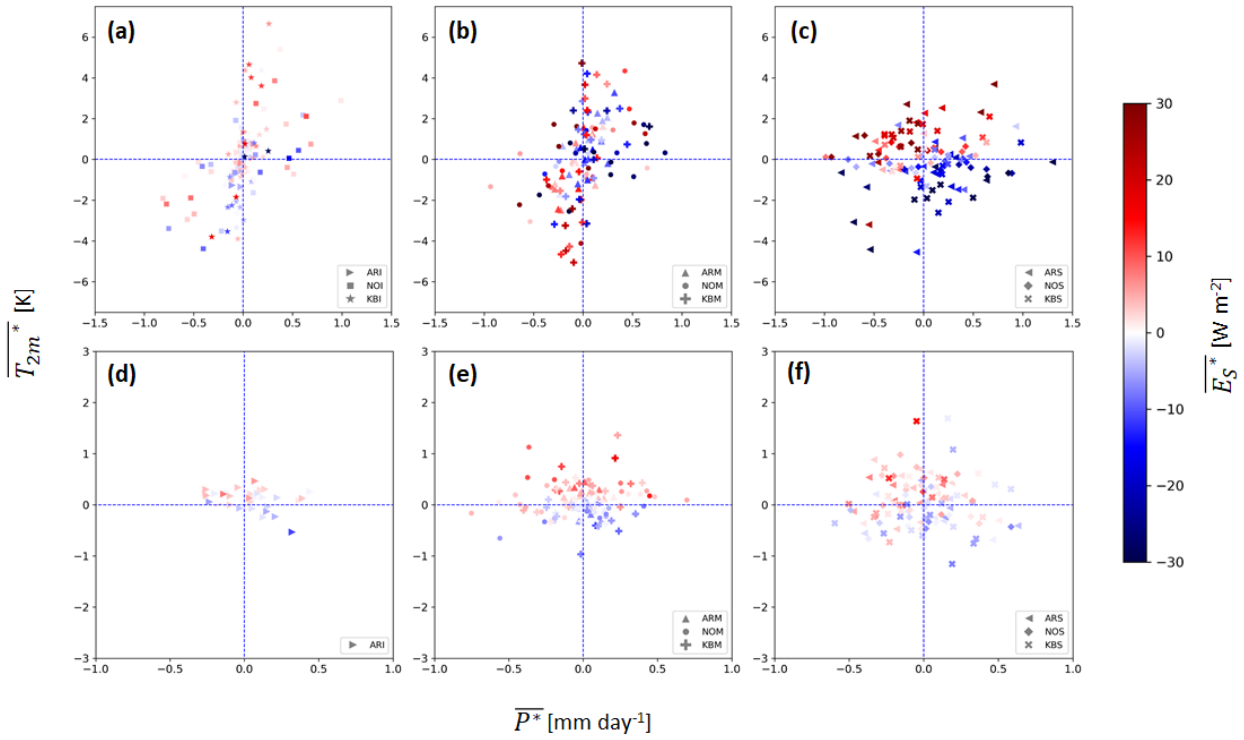

Figure R4: Seasonal-mean anomalies of P ($\overline{P}^*$; mm day^{-1}, along x-axis), T_{2m} ($\overline{T_{2m}}^*$; K, along y-axis) and E_S ($\overline{E_S}^*$; W m^{-2}, color) for 39 seasons in DJF (a,b,c) and JJA (d,e,f) for sub-regions with $SIC_{clim} > 0.9$ (a,d), $0.1 \leq SIC_{clim} \leq 0.9$ (b,e) and $SIC_{clim} < 0.1$ (c,f).

5) l.230: Despite good clustering in Fig. 4, this plot is again very busy. Maybe you can show the average location for each of the nine sub-regions on top of the existing plot.

Thanks for this suggestion. We added averages for each sub-region to Fig. 4 in the revised manuscript (see Fig. R5 below).

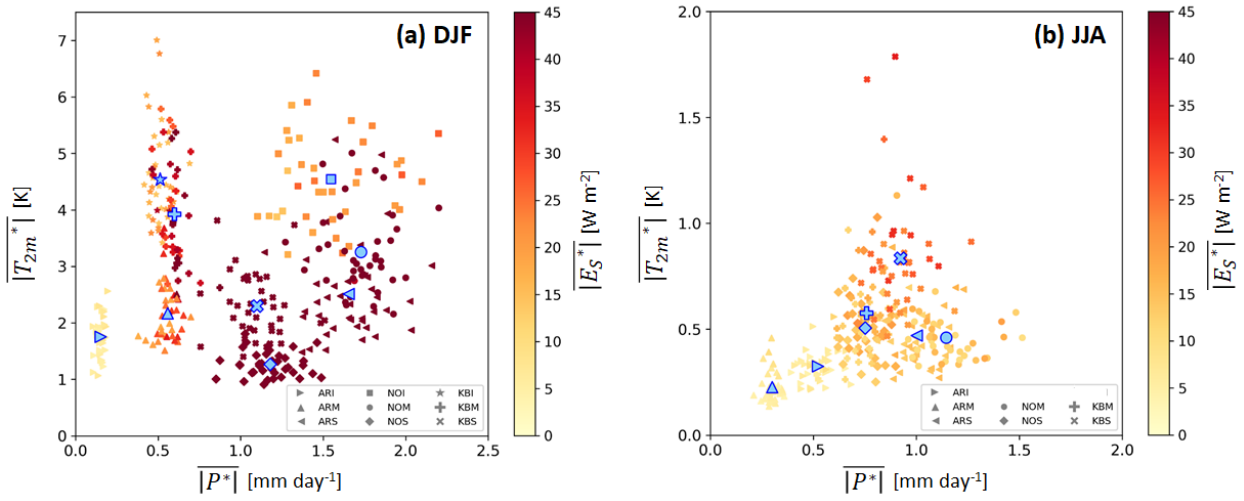

Figure R5: Seasonal-mean absolute anomalies for P ($\overline{|P^*|}$; mm day^{-1} ,along x-axis), T_{2m} ($\overline{|T_{2m}^*|}$; K, along y-axis) and E_S ($\overline{|E_S^*|}$; W m^{-2}, color) for 39 seasons and (a) 9 sub-regions in DJF and (b) 7 sub-regions in JJA. Blue symbols mark average values for each sub-region.

6) Fig.5, 'the seasonal-mean absolute anomalies': are these the seasonal-mean absolute *daily* anomalies, as in Fig. 4?

Yes. We define the seasonal-mean absolute anomalies as the seasonal mean of the absolute daily anomalies (L238ff.), which is valid for all figures in Sect. 3.

7) Fig.5,6: why Nordic seas are not shown?

In order to limit the length of the paper (see also your remark above), we selected some sub-regions for Figs. 5 and 6 (those that are most relevant for the case studies). The other sub-regions are now shown in the Supplement.

8) l.285-287: The statement on correlation between T2m and P comes from the fact that the corresponding blue lines are close to each other?

Yes. The more parallel two precursor vectors are, the stronger is the correlation of the precursors, provided that PC1 and PC2 explain a large part of the variance (Gabriel, 1971; 1972).

9) Regarding the comment on the weather systems creating extremes in the high Arctic, I would like to agree, though none of the AR seasons across all regions in fig. 5 look particularly extreme. How about other regions that have stronger extreme seasons often just in one parameter - can they be explained by anomalous weather patterns?

Yes, we agree, variability is distinctively smaller in the High Arctic in winter. But we think that one strength of our method is that it is still able to objectively quantify the "anomaly magnitude"

of one season compared to another in a specific sub-region. A method using absolute thresholds would find most extreme seasons most likely at the poleward end of the storm tracks.

With respect to your 2nd question, we unfortunately don't understand what you mean by "other regions". For all seasons, which we investigated in detail, we found an important role of anomalous weather patterns.

10) l.303-307: Why the described connection between P and Rs over the sea, as well as between T2m and RL in KBM does not hold in the Kara-Barents Sea?

In **NOS** and **ARS** we can see an anti-correlation between P and R_S (corr(P,R_S)=-0.91 in **NOS** and corr(P,R_S)=-0.96 in **ARS**. Our argument for this anti-correlation is the presence of clouds during rainfall. As you correctly point out, there is no such anti-correlation in sub-region **KBS** (corr(P,R_S)=0.05). This would indicate that there is a large variation in cloud cover (and thus possible reduction in Rs) also during periods without precipitation. We did, however, not investigate this relationship in further detail.

We also want to point out that the mentioned correlations are only an approximation (see previous comment), which is more accurate the more of the total variance is explained by the first two Principal Components. As in the mentioned sub-regions this explained variance ranges between 85% and 88%, we assume that the correlations are good enough to use them for our interpretation.

11) Section 4: The relationship between 6 metrics during cold and warm seasons, gained from the PCA analysis, is interesting. Could correlations found in this section be confirmed by using the raw data?

We are not sure if we understand this question correctly. Yes, we can confirm some of the correlations found with the PCA. For example it is shown in Fig. 3 that in DJF T_{2m} and P are mostly positively correlated in **ice** and **mixed** sub-regions, whereas there is no such correlation in regions over the open ocean. This correlation can as well be seen in the PCA biplots for DJF in Fig. 7. However, as we use six different variables for the PCA analysis, and there seems to be no conventional method to illustrate the correlation of six variables, we only show T_{2m}, P and E_S in Fig. 3. It is further important to mention that we use detrended seasonal-mean anomalies for the PCA and thus remove the seasonality and a potential trend compared to the raw data. Therefore, it is not straightforward to compare the correlation of certain parameters for both data sets.

12) l. 322: "By design, extreme seasons have very large anomalies for at least one parameter… However, some anomalous seasons don't show very strong anomalies in one particular parameter, which implies that for these seasons it is the combination of several parameters that makes them anomalous" I am not sure that the first sentence is true. Moderate anomalies in a few variables may also give an anomalous season and this is what happens in some cases.

Thank you for this remark. We rephrased the mentioned section (L349ff.) in order to clarify that indeed our **extreme** seasons have at least one large anomaly in one parameter (see previous

comment about the approach as well as answer to comment 1 by the Editor) to reach a d_M value which is larger than 3. However, it is correct that this is not necessarily the case for **anomalous** seasons, where it is often the combination of several moderate anomalies resulting in d_M>2 (but smaller than 3).

13) l.367: I could not find a description of how cyclones, CAO and blocking events were defined.

For the specifics of the identification scheme, we added a few sentences for each weather system and now give the relevant references to the papers that introduced these schemes (L132ff., see answer to specific comment (9) by reviewer 1).

14) l.372: Even during CAOs the temperature remained above the climatological mean, hence, I doubt that 38%-deficit in CAO can be responsible for the season being anomalous. During the first month (days1-27), there were no significant blocking events and CAOs, but T2m was well above average. To me it looks like there was a strong preconditioning. Furthermore, in the next case, shown in Fig. 10, there is a high number of CAOs but they have relatively small effect on T2m, especially during the first half of the season, brings the temperature down by only, perhaps, 2-3 deg.

Thank you for this remark, it is certainly important to discuss this more thoroughly. As we state in section 5.3, where we discuss the synoptics throughout the winter 2011/12, one important feature is the pathway of the cyclones entering the Arctic from the North Atlantic, as they tend to slow down and get stationary in the region of the Nordic Seas, and their position relative to the Kara and Barents Seas. As a result, during several days of this winter, the warm sector of a cyclone is located in the Kara and Barents Seas whereas its cold sector is positioned in the Nordic Seas. This does not only explain partially the relative lack of CAOs, but also the overall increase in the surface temperature anomaly. If the cyclones were located further east, both the warm and the cold sectors would have been located in the region, likely resulting in no notable T_{2m} anomaly. Comparing the timeseries in Fig. 9 with the supplementary animation S1 shows that this synoptic situation especially occurs in December and in the second half of February, when the T_{2m} anomaly is very strong. For further studies it could thus be very useful to have a metric for the coverage of a region by a cyclones' warm sector as opposed to its cold sector (and thus the position of a cyclone with respect to that region). This would simplify the interpretation of a cyclones' influence on surface parameter anomalies in a distinct region. In the revised manuscript we now emphasize more that the impact of cyclones depends critically on their track relative to the region (L500ff.).

With regard to your comment on preconditioning in this season, we can say that this is most probably only a minor reason for the anomalous surface temperatures. Indeed, SON 2011 shows already slightly positive $\overline{T_{2m}}^{*}$ values and a slightly reduced SIC, but not to an extent that could explain the strong seasonal-mean T_{2m} anomaly during DJF 2011/12. The sea surface temperature reaches values of about +1-1.5 K above normal in September 2011, however returns to climatological values in October and shows no significant anomalies throughout November.

15) l.465: A seasonal blocking anomaly over Scandinavia is probably not enough to support the statement that 'Subsidence-induced warming [over Scandinavia] and long-range transport of warm air masses contributed to several warm episodes.'

This is indeed correct. To confirm this statement, we added a short evaluation of some air parcel trajectories to the supplement, which show the importance of subsidence-induced warming and long-range transport during episodic warm events in DJF 2016/17.

Figure R6 shows air parcel trajectories for two warm episodes in DJF 2016/17 from 16-19 January 2017 (Fig. R6a) and from 11-14 February 2017 (Fig. R6b). In January, the influence of long-range transport of air parcels at lower levels, mainly from eastern Europe, can be observed. In February, subsiding air masses, favored by the presence of a blocking system over Scandinavia, additionally contribute to the warm event.

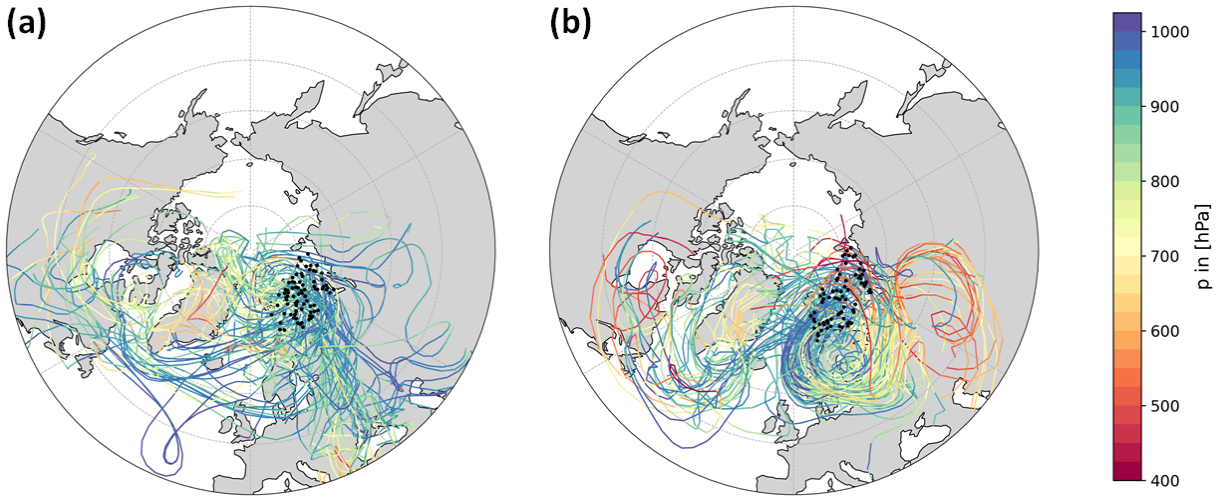

Figure R6: 10-day kinematic backward trajectories associated with positive daily mean T_{2m} anomalies in the region of the Kara and Barents Seas for the period (a) 16-19 January 2017 and (b) 11-14 February 2017 colored according to pressure. Trajectories are initialized every 6 hours at 25, 50, 75 and 100 hPa above ground for grid points with $T_{2m}^{*} \geq 2\,K$. Every 100th trajectory is shown with black dots denoting the starting point of each trajectory.

16) l.498: why a persistent high does not cause subsidence warming? and why there are no blocking events during Jan 2013 at the time of a persistent high? I can also see a number of cyclones in Feb, despite the text says that Feb was also calm. I agree that probably the main reason for decreasing t2m and low P is that the High Arctic remained isolated from the lower latitudes, however, none of the metrics in this study reflect an exchange between latitudes. I am not suggesting adding such metric at this stage, but it might be something to add in the future.

Thank you for these remarks. It would certainly be useful to have a measure which is indicative for latitudinal air mass exchange to better understand the processes leading to extreme seasons in the High Arctic.

Regarding your questions about the non-co-occurrence of the persistent high-pressure system as well as the lack of subsiding air, we analysed the geopotential height as well as the potential vorticity (PV) anomaly at upper levels throughout this winter. Figure R7 shows the geopotential height at 300 hPa (Z300) during the episode of the strong high-pressure system between 15 January and 25 January 2013 in the region of the Chukchi Sea and the High Arctic. Z300 does not show significantly enhanced values above the surface high, indicating that there is no strong upper-level forcing in the form of a persistent ridge which could have caused the formation of a block and the strong subsidence of air. The analysis of the vertically averaged potential vorticity anomaly (VAPVA) between 500 and 150 hPa does further support these results, as it reaches only small negative or even positive values in the same region (for the identification of a block following Sprenger et al. (2017), an area with VAPVA < -1.3pvu which persists for at least 5 days would be needed). Thus we assume that the strong high-pressure system at the surface is caused by very cold air below an inversion layer, decoupled from the synoptics in the upper troposphere. We can show that there exists a strong inversion layer very close to the surface in the center of the high pressure system by using a skew*T*-log*P* diagram (see Fig. R8), which supports our assumption that the air in this area experiences radiative cooling opposed to subsidence-induced adiabatic warming which one might expect in the presence of an upper-level block.

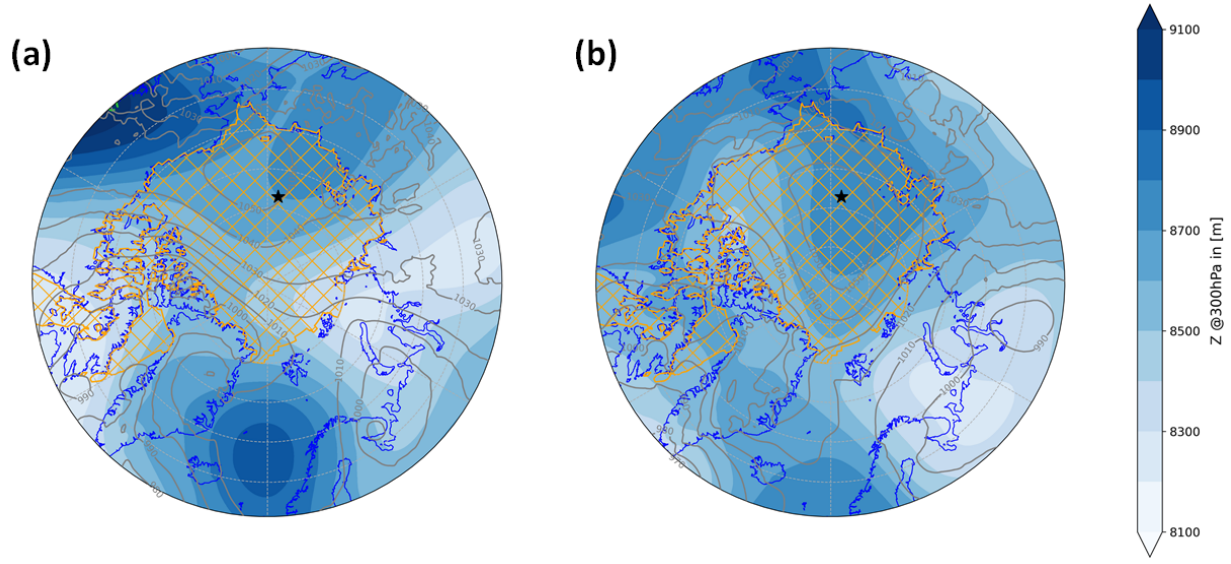

Figure R7: Synoptic situation on (a) 20 January 2013 and (b) 24 January 2013. Daily mean geopotential height at 300 hPa (in hPa, color). Sea level pressure (grey contours, in intervals of 10 hPa) and blocking mask (dashed green contour) at 00 UTC on the considered days. Black star at 173°E, 78.5°N shows location of skew*T*-log*P* profile in Fig. R8. Sub-region **ARI** is marked by orange hatching.

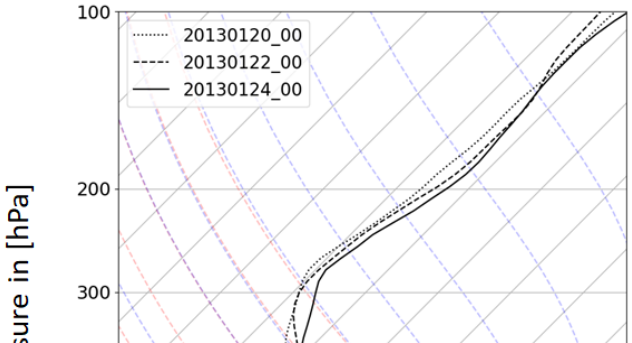

Figure R8: Skew*T*-log*P* diagram 173°E, 78.5°N (black star in Fig. R7). Temperature is shown along the x-axis (in °C) and pressure along the y-axis (in hPa). Black lines show the ambient

temperature profile for 20 January 2013 (dotted line), 22 January 2013 (dashed line), and 24 January 2013 (solid line) at 00 UTC. Grey lines show isobars (horizontal) and isotherms (skewed), respectively. Colored dashed lines denote dry (red) and moist (blue) adiabats, respectively. Green dotted lines denote constant saturation mixing ratios.

We replaced Fig. 15 from the first manuscript with Figs. R7 (Fig. 15) and R8 (Fig. 16) and adapted lines 544ff. in the revised manuscript to clarify the synoptics during DJF 2012/13.

17) l.529-534: the paragraph first describes obvious seasonal differences (higher variability in winter due to stronger gradients) and then concludes 'hence, it is reasonable to subdivide the Arctic into several regions considering these spatial differences to study anomalous Arctic winter seasons.' But during summer the regions were also subdivided. I am not sure if this paragraph is needed at all.

Thank you very much for this remark. The mentioned paragraph is indeed a bit misleading and possibly not needed at all, which is why we deleted it. However, we still want to mention the difference in spatial variability between winter and summer and therefore added a sentence in this regard to the previous paragraph (L568).

18) l. 541: see my major comment on the PCA approach

See our response on p.12 of this reply document.

Minor comments:

1) l.61 'and of the feedback': remove 'of'

Changed "strongly affect the type of linkages between parameters and of the feedback processes" to "strongly affect the type of linkages between parameters as well as feedback processes".

2) Table 1: Es should be added

Thank you for pointing this out, we added the variable "*Es*" to Table 1.

3) Table 2 is first mentioned in section 2.3 but is only shown in section 4. Replace 'brackets' with 'parentheses'

Thank you, we changed "brackets" to "parentheses" in the Table caption.

Indeed we refer to Table 2 already in the method part to justify the detrending of our data set. However we prefer to show Table 2 only in the results part and not yet in the methods part as it basically shows the results of our analysis, based on the PCA biplots in Figs. 7 and 8.

4) l.160: it is not the entire ERA5 period, but the entire period covered by this paper

Thank you for pointing this out. We changed the regarding sentence to “A distinction is made between areas where, on all days of the considered season in the time period covered by this study, mainly sea ice is present …”.

5) Please use either the Kara-Barents sea or the Kara and Barents seas

We now only use “Kara and Barents Seas”.

6) 406: I’d replace ‘single’ with ‘individual’

We replaced “single” by “individual”.

7) 432: on this date

Thank you, changed as requested.

8) Fig. 13 is mentioned earlier than fig. 12.

We rephrased the mentioned part in line 474, to clarify that we only refer to section 5.3 here and not yet want to discuss Fig. 13.

9) Fig. 10,11, 14: I suggest showing months and days of months’ along Axis X, instead of days of season, as specific dates are often mentioned in the text (e.g, 9 Jan or 17 Feb). Can SLP be added to fig. 10,11? In fig. 14 the legend mentions CAOs, but they are not shown - could they be added?

Regarding days/dates: see our answer to specific comment (8) of Reviewer 1.

We added SLP to Figs. 10 and 11. Further we removed the CAO heatmap description from the caption. It does not make sense to show the marine air outbreak frequency for sub-region **ARI**, as this region is mainly ice-covered and as mentioned in the method section (L139ff.), we define CAOs only for grid points with a sea ice concentration of less than 50%.

Reviewer 3

The authors have investigated seasonal extremes in the Arctic using PCA of six climate variables and analysis of some key dynamical elements – cyclones, blockings, and marine cold air outbreaks – to further investigate particular extreme seasons. This is an interesting and valuable framework for understanding the various causes of seasonal extremes, and it is very well presented. I recommend the manuscript for publication with some minor adjustments. My principal concerns relate to the justification of the many choices which needed to be made in this analysis, these are detailed below.

Specific comments:

1) L13: “respectively” – this doesn’t quite follow when you say 2-3 extreme seasons for four seasons.

Thank you, we changed the wording to “...our approach identifies 2-3 extreme seasons for each of winter, spring, summer and autumn, with strongly differing characteristics…”.

2) L15: I think a justification of why 2 winter seasons were chosen for the in-depth case studies is needed here.

See answer to general remark (4) by reviewer 1.

3) L117: It is very nice to have these questions in the Introduction to frame the paper, but as far as I could see the synoptic systems of interest are pre-defined in the study (cyclones, blockings, and marine CAOs), so perhaps this question should be reframed to reflect this.

This is indeed a good point. We rephrased question 3: “In which way do synoptic-scale weather systems such as cyclones, blocks and marine cold air outbreaks determine the sub-structure of extreme seasons?”

4) L131: What was the method(s) of interpolation?

This interpolation is done by the ECMWF software when downloading the ERA5 fields from the MARS archive.

5) L155: What is the justification for choosing these regions?

As stated, a distinction between areas with differing sea-ice concentration is made, as surface heat fluxes and surface radiation are strongly dependent on the surface conditions. Further, we defined three different geographical regions, namely the Nordic Seas (**NO**), the Kara and Barents Seas (**KB**) and the remaining Arctic (**AR**). These are chosen based on the following main features: The **NO** region is the endpoint of the Atlantic storm track and important for deep water formation. The **KB** region has been strongly affected by changes in sea ice concentration and reacts very sensitively to atmospheric forcing. It is also a preferred region for atmospheric blocking and has its “own” storm track. Region **AR** is largely uncoupled from the mid-latitudes. Due to these different characteristics, it is useful to look at these regions separately when analysing the dynamical processes leading to Arctic extreme seasons. We added a sentence in this regard to the manuscript (L160ff.) to further justify the choice of our regions.

6) L161: Are results sensitive to the choice of definition of ice, mixed, and sea? Why were these thresholds chosen?

The results are sensitive to the choice of the SIC thresholds when defining ice, mixed and sea, because obviously the resulting regions get larger or smaller depending on how the thresholds are changed. For instance, if for ice, the threshold SIC_{clim} was lowered from 0.9 to 0.8 then this

would increase the size of the ice regions (and decrease the size of the mixed regions) and therefore the results for ice and mixed would be slightly less distinct. We decided to use relatively strict thresholds for ice and sea to ensure that these regions are indeed almost completely ice-covered and ice-free, respectively.

7) L174: Why choose just the first 2 PCs? This seems arbitrary, although I see later you mention that these explain a very large part of the overall variance.

See answer to first general comment of Reviewer 1. And yes, indeed the first two Principal Components explain usually 80-90% of the overall variance (in more detail: in 88% of the cases its >80% explained variance, in 53% of the cases they explain even >85% of the overall variance) and they are - for almost all regions and seasons - statistically distinct.

8) L178: Why are these rescaled by their respective SDs to give equal weight to each PC? Do you not wish to identify the extremeness of a season rather than the extremeness of a season with respect to these two PCs? (ref L114) If you don't do this rescaling do you still identify the same seasons as being extreme seasons?

We decided to use the scaled Euclidean distance (= Mahalanobis distance) in the PCA phase space to define our extreme seasons as with this approach, outliers in both, PC1 and PC2, are considered equally (without the rescaling, there would be more weight on the PC1 outliers). Thus, outliers in both PCs are treated similarly, independent of the individual variance explained by each PC.

We haven't tested the identification of extreme seasons without rescaling. Without rescaling, different, subjective thresholds for the definition of anomalous and extreme seasons would have to be chosen, which would hamper a direct comparison of the two methods.

9) Fig 8 and elsewhere: why was 10^5 km^2 chosen as the size threshold for a region?

This is a very pragmatic and subjective choice. Results from a PCA might be less reliable for very small regions. With this threshold, each region comprises at least 40 model grid points.

10) L393: grammar – "This periods typically are…"

Thank you, changed as suggested.

11) L408: "exemplarily shows" -> "exemplifies"

Thank you, changed as suggested.

12) L510: "as is the case"

Thank you, changed as suggested.

References:

Gabriel, K. R.: The biplot graphic display of matrices with application to principal component analysis, Biometrika, 58, 453–467,https://doi.org/https://doi.org/10.2307/2334381, 1971.

Gabriel, K. R.: Analysis of Meteorological Data by Means of Canonical Decomposition, J. Appl. Meteorol., 11, 1071–1077, https://doi.org/https://doi.org/10.1175/1520-0450(1972)011<1071:AOMDBM>2.0.CO;2, 1972.

North, G. R., T. L. Bell, R. F. Cahalan, and F. J. Moeng, Sampling errors in the estimation of empirical orthogonal functions. Mon. Wea. Rev., 110, 699-706, http://dx.doi.org/10.1175/1520-0493(1982)110%3C0699:SEITEO%3E2.0.CO;2, 1982.

Röthlisberger, M., Hermann, M., Frei, C., Lehner, F., Fischer, E. M., Knutti, R., and Wernli, H., A new framework for identifying and investigating seasonal climate extremes, J. Clim. (published online ahead of print 2021). Retrieved Jul 9, 2021, from https://journals.ametsoc.org/view/journals/clim/aop/JCLI-D-20-0953.1/JCLI-D-20-0953.1.xml, 2021.

Sprenger, M., Fragkoulidis, G., Binder, H., Croci-Maspoli, M., Graf, P., Grams, C. M., Knippertz, P., Madonna, E., Schemm, S., Škerlak,B., and Wernli, H.: Global climatologies of Eulerian and Lagrangian flow features based on ERA-Interim, B. Am. Meteorol. Soc., 98,1739–1748, https://doi.org/10.1175/BAMS-D-15-00299.1, 2017.

Tyrlis, E., Manzini, E., Bader, J., Ukita, J., Nakamura, H., and Matei, D.: Ural blocking driving extreme Arctic sea ice loss, cold Eurasia, and stratospheric vortex weakening in autumn and early winter 2016–2017, J. Geophys. Res.: Atmos., 124, 11 313–11 329, https://doi.org/10.1029/2019JD031085, 2019.

Identification, characteristics, and dynamics of Arctic extreme seasons

Katharina Hartmuth[1], Maxi Boettcher[1], Heini Wernli[1], and Lukas Papritz[1]

[1]Institute for Atmospheric and Climate Science, ETH Zurich, Zurich, Switzerland

Correspondence: Katharina Hartmuth (katharina.hartmuth@env.ethz.ch)

Abstract.

The Arctic atmosphere is strongly affected by anthropogenic warming leading to long-term trends in, e.g., surface temperature and sea ice extent. In addition, it exhibits a pronounced seasonal cycle and strong variability on time scales from days to seasons. Recent research elucidated processes causing short-term extreme conditions in the Arctic that are typically related to the occurrence of specific weather systems. This study investigates unusual atmospheric conditions in the Arctic on the seasonal time scale, characterized by surface temperature, ~~surface~~ precipitation, and the atmospheric components of the surface energy balance. Based on a principle component analysis in the phase space spanned by the seasonal-mean values of the considered parameters, individual seasons are ~~then~~ objectively identified that deviate strongly from a running-mean climatology, and that we define as extreme seasons. Given the strongly varying surface conditions in the Arctic, this analysis is done separately in Arctic sub-regions that are climatologically characterized by either sea ice, open ocean, or mixed conditions.

Using ERA5 reanalyses for the years 1979-2018, our approach identifies 2-3 extreme seasons for each of winter, spring, summer, and autumn, ~~respectively,~~ with strongly differing characteristics and affecting different Arctic sub-regions. While some show strongly anomalous seasonal-mean values mainly in one parameter, others are characterized by a combination of ~~very~~ unusual seasonal conditions in terms of temperature, precipitation, and the surface energy balance components. Two extreme winters affecting the ~~Kara-Barents Seas are then~~ Kara and Barents Seas are selected for a detailed investigation of ~~(i)~~ their substructure, ~~(ii)~~ the role of synoptic-scale weather systems~~that occur during the season, and (iii)~~ , and potential preconditioning by anomalous sea ice extent and/or sea surface temperature at the beginning of the season. Winter 2011/12 ~~shows the highest surface temperature anomaly in parts of the Kara-Barents Seas (about + 5 K), which was due to~~ started with normal sea ice coverage and was characterized by constantly above-average temperatures during the season related to a ~~strongly~~ sequence of quasi-stationary cyclones in the Nordic Seas, favoring the frequent advection of warm air to the Barents Sea. An enhanced frequency of blocking anticyclones ~~in the Kara-Barents Seas and a strongly~~ and a reduced frequency of cold air outbreaks ~~. Sea ice coverage was normal at the beginning of the season and then developed a negative anomaly due to the unusually high temperatures~~in the Kara and Barents Seas further helped to maintain the warm anomaly. In contrast, winter 2016/17 started with a strongly ~~negative anomaly in~~ reduced sea ice coverage and ~~a strongly positive anomaly in sea surface temperature in the Kara-Barents Seas, which remained during most of the season. The combination of this preconditioningwith specific synoptic conditions, i.e., a particularly high frequency~~ enhanced sea surface temperatures in the Kara and Barents Seas. This

preconditioning, together with increased frequencies of cold air outbreaks and ~~an increased frequency of~~ cyclones, was responsible for the ~~extreme characteristics of this season, reflected in~~ large upward surface heat flux anomalies and strongly increased precipitation during this extreme season.

In summary, this study shows that extreme seasonal conditions in the Arctic are spatially heterogeneous, related to different near-surface parameters, and caused by different synoptic-scale weather systems, potentially in combination with surface preconditioning due to anomalous ocean and sea ice conditions at the beginning of the season. The framework developed in this study and the insight gained from analyzing the ERA5 period will be beneficial for addressing the effects of global warming on Arctic extreme seasons.

1 Introduction

Near-surface atmospheric conditions in the Arctic show a high variability on synoptic to inter-annual temporal scales, which is superimposed on a strong, long-term warming trend ~~(e.g. Serreze and Barry, 2011; Cohen et al., 2014)~~(e.g., Serreze and Barry, 2011; Cohe
Key drivers of variability on the synoptic to weekly time scale are interactions with the mid-latitudes for instance via air mass exchanges ~~(e.g. Woods et al., 2013; Laliberté and Kushner, 2014; Graversen and Burtu, 2016; Messori et al., 2018; Papritz and Dunn-Sige~~ air mass transformations within the Arctic (Ding et al., 2017; Pithan et al., 2018; Papritz, 2020). Both air mass exchanges and transformations are found to be related to synoptic weather systems. On longer time scales, in contrast, memory effects and feedback mechanisms such as the sea ice albedo feedback (Arrhenius, 1896; Curry et al., 1995), the water vapor and cloud feedbacks (Vavrus, 2004; Graversen and Wang, 2009; Boisvert et al., 2016), as well as the temperature feedback (Pithan and Mauritsen, 2014) play an important role. Given this broad spectrum of processes, this leads to the question how variability on various temporal scales is inter-connected. In this study, we focus on the seasonal scale and it is our goal to analyze the role of intra-seasonal processes, including synoptic-scale weather systems, for the emergence of seasonal extremes in the Arctic. The following paragraphs provide the relevant background on the key near-surface meteorological parameters in the Arctic and how they are interrelated. Furthermore, we discuss the role of different synoptic-scale weather systems for the variability of these parameters and the occurrence of short-term extremes and seasonal anomalies in the Arctic.

Near-surface temperature, the components of the surface energy budget - including radiative and turbulent heat fluxes - as well as surface precipitation are especially important parameters linking the variability of the atmosphere with that of the ocean and the cryosphere. Large fluctuations in the surface energy budget, which themselves are closely linked to air temperature fluctuations, contribute to the variability of sea ice (Stroeve et al., 2008; Olonscheck et al., 2019), the ocean mixed layer as well as open ocean convection ~~(e.g. Marshall and Schott, 1999)~~(e.g., Marshall and Schott, 1999). Radiative and sensible heat fluxes drive the variability of the surface energy budget components over sea ice (Lindsay, 1998), whereas over open ocean turbulent heat fluxes dominate (Segtnan et al., 2011). Precipitation variability influences snow cover, which is strongly linked to the albedo feedback, and it affects the freshwater balance of the Arctic Ocean and the Nordic Seas (Serreze and Francis,

2006; White et al., 2007), which jointly with turbulent heat fluxes impacts the thermohaline circulation (Dickson et al., 1996; Talley, 2008).

The three parameters - near-surface temperature, surface energy budget, and surface precipitation - do not vary independently from each other but they are interlinked. Thereby, the surface boundary conditions, i.e., sea ice vs. open ocean, strongly affect the type of linkages between parameters ~~and of the~~ as well as feedback processes due to vastly different heat capacities. On synoptic time scales, for instance, warm and cold air advection strongly influence heat fluxes over the open ocean, where the most intense upward fluxes occur in cold air outbreaks (Harden et al., 2015; Papritz and Spengler, 2017; Pope et al., 2020). On longer time scales, surface air temperature changes are largely influenced by variations in the sea surface temperature via surface sensible heat fluxes (Johannessen et al., 2016). In addition, incoming shortwave radiation is absorbed and can be released to the atmosphere later. Over sea ice, in contrast, temperature is to a large degree determined by the surface energy balance, which includes radiative and turbulent heat fluxes, conductive heat fluxes across the ice and latent energy for freezing and melting (Serreze and Francis, 2006). In winter, when the incoming shortwave radiation is strongly reduced, the surface sensible heat flux and net surface longwave radiation mainly determine the surface energy balance in regions covered by sea ice (Ohmura, 2012). These considerations reveal that a meaningful identification of extreme seasons in terms of the surface temperature, energy budget and precipitation parameters must take their co-variability and the underlying surface boundary conditions into account.

The role of synoptic-scale weather systems for inter-annual variability in the Arctic has been subject of multiple recent studies, which emphasized especially the importance of cyclones (Simmonds and Rudeva, 2012; Messori et al., 2018), blocking anticyclones (Wernli and Papritz, 2018; Papritz, 2020), and Rossby wave breaking (Liu and Barnes, 2015). Air mass exchanges between the mid-latitudes and the Arctic region are often facilitated by cyclones, which, on one hand, transport warm and moist air to higher latitudes (Sorteberg and Walsh, 2008; Messori et al., 2018), causing there an increase in downward heat fluxes as well as the formation of clouds and precipitation. On the other hand, the advection of cold and dry air in the cyclones' cold sector enhances ocean evaporation and heat fluxes into the atmosphere. Additionally, extreme moisture transport into the Arctic is often associated with events of Rossby wave breaking (Liu and Barnes, 2015), which can be strongly linked to the evolution of surface cyclones (Martius and Rivière, 2016). Air mass transformations within the Arctic can similarly result in anomalous conditions. Recent studies emphasized the importance of polar anticyclones and blocking events in the High Arctic, driving subsidence-induced adiabatic warming and thus leading to anomalies in surface temperature and net surface radiation, resulting in increased sea ice melting (Wernli and Papritz, 2018; Papritz, 2020). In winter, radiative heat loss under clear-sky conditions can lead to extreme cold conditions, whereas cloud formation favors the trapping of longwave radiation, thus providing a positive warming feedback and causing an increase in surface temperature (Boisvert et al., 2016; Woods and Caballero, 2016). Similarly, a persistent and strong tropospheric polar vortex over the pole can isolate polar air masses and result in anomalously cold conditions due to enhanced radiative cooling (Messori et al., 2018; Papritz, 2020). Therefore, air mass transport and air mass transformation can significantly influence the Arctic surface energy balance. Whereas the modification of turbulent heat

fluxes is of particular importance over the open ocean, the impact on radiative fluxes, for instance due to an increase in the atmospheric moisture content, is highly relevant in regions covered by sea ice.

Several studies have analyzed short-term Arctic extreme events and the involved dynamical processes, for instance the unusual warm event in winter 2015/16, which led to above freezing temperatures close to the North Pole (Cullather et al., 2016) and caused significant sea ice melting in the ~~Kara-Barents~~ Kara and Barents Seas (Boisvert et al., 2016). Binder et al. (2017) were able to show that several pathways of exceptional air mass transport caused this warm event. Another example is an extreme melt event on the Greenland ice shield in July 2012 (Nghiem et al., 2012), which was found to be related to a blocking anticyclone and associated anomalous long-range transport of warm and humid air masses from the South (Hermann et al., 2020). Such extreme weather events can have significant long-term effects, particularly due to their impact on sea surface temperatures and sea ice extent. For instance, Simmonds and Rudeva (2012) have shown that a particularly intense Arctic cyclone in summer caused the dispersion and separation of sea ice, leaving the main sea ice pack more exposed and thus vulnerable to further melting. Similarly, the described extreme warm event in December 2015 caused positive anomalies in sea surface temperature and negative anomalies in sea ice concentration in the ~~Kara-Barents~~ Kara and Barents Seas, which persisted throughout the year 2016 (Blunden and Arndt, 2017). Single events of extreme weather, causing episodes of strongly anomalous conditions such as exceptionally high or low surface temperatures, can thus have a major impact on seasonal-mean surface temperature, the formation and melting rates of sea ice, and on minimum and maximum sea ice extent.

Despite these insights, so far only little attention has been given to systematically understanding the characteristics of extreme seasonal-mean conditions in the Arctic, and the role of synoptic weather systems in their formation. Therefore, our study aims to address the following research questions:

1. How spatially (in)homogeneous are the seasonal-mean near-surface atmospheric conditions in the Arctic in winter and summer?

2. How can extreme seasons be defined objectively, based on a combined analysis of different key surface parameters in Arctic sub-regions?

3. ~~Which dynamical processes, in particular, which~~ In which way do synoptic-scale weather systems such as cyclones, blocks and marine cold air outbreaks determine the sub-structure of extreme seasons?

4. What is the role of surface preconditioning , i.e., of early season anomalies of sea surface temperature and/or sea ice concentration for the formation of extreme seasons?

To address these research questions, a novel method will be introduced to determine the “unusualness" of a season, which we define based on a combination of various surface parameters. Our study is organized as follows: Data and methods are described in Section 2. Section 3 presents an overview of the seasonal variability of surface temperature, surface precipitation, and of the surface energy budget components. In Section 4 we define anomalous and extreme seasons in the Arctic based on

seasonal anomalies of these parameters, and analyze their substructure in distinct Arctic sub-regions. Detailed analyses of three Arctic extreme seasons and the involved atmospheric synoptic-scale processes are presented in Section 5, followed by the main conclusions in Section 6.

2 Data and ~~method~~methods

2.1 ERA5 data

To perform a detailed analysis of Arctic extreme seasons, the ERA5 reanalysis dataset of the European Centre for Medium-Range Weather Forecasts (ECMWF) is used (Hersbach et al., 2020). Hourly atmospheric fields and short-range forecasts were spatially interpolated to a $0.5° \times 0.5°$ horizontal grid on model levels. The study period includes winters [December-February (DJF)] from 1979/80 to 2017/18 as well as springs [March-May (MAM)], summers [June-August (JJA)] and autumns [September-November (SON)] from 1980 to 2018. Based on the ERA5 dataset, we additionally consider synoptic features such as extratropical cyclones and blocks identified following the methods presented in Sprenger et al. (2017). Here, cyclones are defined as objects covering the area around a sea level pressure minimum, delimited by the outermost closed sea level pressure contour (Wernli and Schwierz, 2006). Blocks are identified based on the deviation of vertically averaged potential vorticity between 150 and 500 hPa from the monthly climatological mean. Contiguous areas where this value falls below -1.3 pvu are tracked in time and tracks that persist for at least 5 days are considered as blocks (Schwierz et al., 2004; Croci-Maspoli et al., 2007).

Further, we define cold air outbreaks (CAOs) based on the exceedance of the 900 hPa sea-air potential temperature difference ($\theta_{SST} - \theta_{900}$) by +4 K (cf. Papritz and Spengler, 2017), whereby we exclude grid points over land or with a sea ice concentration of more than 50 %. As outlined below, particularly anomalous seasons are identified based on seasonal-mean anomalies of the following six variables in specific regions: 2 m temperature (T_{2m}), precipitation (P, defined as the sum of convective and large-scale precipitation), surface sensible heat flux (H_S), surface latent heat flux (H_L), net surface shortwave radiation (R_S) and net surface longwave radiation (R_L). The last four variables are relevant for the surface energy balance and their sum is denoted by E_S. Positive signs denote energy fluxes into the surface, whereas negative signs are indicative for energy fluxes into the atmosphere. We use short-range forecasts for the fluxes P, H_S, H_L, R_S and R_L and analyses for the other fields.

Abbreviation	Variable name	Unit
		[W m^{-2}]
E_S	sum of H_S, H_L, R_S and R_L	
	surface latent heat flux	[W m^{-2}]
H_L		
H_S	surface sensible heat flux	[W m^{-2}]
P	precipitation	[mm day^{-1}]
R_L	net surface longwave radiation	[W m^{-2}]
R_S	net surface shortwave radiation	[W m^{-2}]
SIC	sea ice concentration	
SST	sea surface temperature	[K]
T_{2m}	2 m temperature	[K]

Table 1. List of variable names used in this study.

To compute anomalies, a transient climatology is calculated at every grid point as follows. First, daily-mean values of the variables are smoothed with a 21-day running mean filter. In a second step, the 9-year running mean is computed for each calendar day. Thus, the seasonal cycle is retained in the climatology, but decadal variations and long-term trends related to the overall warming of the Arctic are removed. The climatology is kept constant at the beginning and end of the study period when no 9-year running mean can be calculated. Examples of this filtering procedure are shown in the supplementary material, where Fig. S1a and b shows the original T_{2m} time series in the ~~Kara-Barents~~ Kara and Barents Seas and illustrates that the 9-year running mean can effectively eliminate also non-linear long-term trends (T_{2m} in the ~~Kara-Barents~~ Kara and Barents Seas steeply increases in the decade from 2000-2010). Seasonal-mean anomalies are then defined as deviations of the seasonal-mean values from this transient climatology. With this approach (also used by Messori et al. (2018) and Papritz (2020)), the identified extreme seasons appear relatively uniform throughout the study period (see Table 2 and Tables ~~S1-S4~~ S3-S6 in the supplementary material). Throughout the study, we denote daily anomalies of a variable χ as χ^*, seasonal-mean anomalies as $\overline{\chi^*}$ and seasonal-mean absolute anomalies as $\overline{|\chi^*|}$.

2.2 Definition of sub-regions

~~It is one goal of this study to analyze the characteristics of Arctic extreme seasons with respect to climatological conditions. Therefore, extreme seasons~~ Extreme seasons will be identified in three distinct geographical regions, the Nordic Seas (**NO**), ~~the Kara-Barents~~ endpoint of the Atlantic storm track (e.g., Wernli and Schwierz, 2006) and area of deep water formation (e.g., Dickson et al., 1996), the Kara and Barents Seas (**KB**), which are strongly affected by recent changes in sea ice concentration (e.g., Cavalieri and Parkinson, 2012), and the remaining Arctic poleward of 60° N (**AR**, containing the ~~High Arctic region > 80° N)~~Arctic Ocean), which is to some extent dynamically de-coupled from the mid-latitudes. Grid points above land are excluded. It is one goal of this study to analyze the characteristics of Arctic extreme seasons with respect to climatological

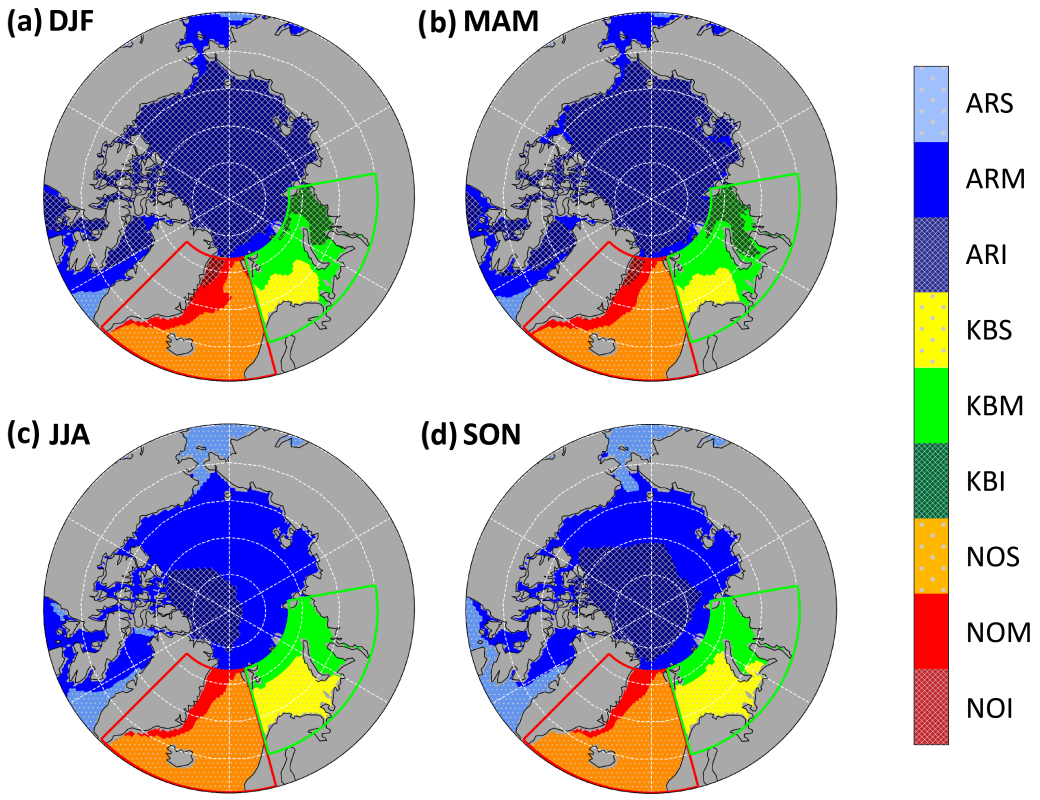

Figure 1. Sub-regions defined based on SIC_{clim} in **(a)** DJF, **(b)** MAM, **(c)** JJA, and **(d)** SON. The labels refer to: **NOI**: Nordic Seas Ice, **NOM**: Nordic Seas Mixed, **NOS**: Nordic Seas Sea, **KBI**: ~~Kara-Barents~~ Kara and Barents Seas Ice, **KBM**: ~~Kara-Barents~~ Kara and Barents Seas Mixed, **KBS**: ~~Kara-Barents~~ Kara and Barents Seas Sea, **ARI**: Arctic Residual Ice, **ARM**: Arctic Residual Mixed, **ARS**: Arctic Residual Sea. Green and red boxes denote the areas of the Kara and Barents Seas and Nordic Seas regions, respectively.

conditions. As the variables, especially the surface heat fluxes and surface radiation are strongly dependent on the surface conditions ~~(e.g. Pope et al., 2020)~~(e.g., Pope et al., 2020), the regions are additionally subdivided in each season according to the climatological seasonal-mean sea ice concentration (SIC_{clim}). A distinction is made between areas where, on all days of the considered season in the ~~entire ERA5 time period~~ time period covered by this study, mainly sea ice is present (**Ice**, $SIC_{clim} > 0.9$), mainly open ocean is present (**Sea**, $SIC_{clim} < 0.1$), and regions of intermediate SIC_{clim} (**Mixed**, $0.1 \leq SIC_{clim} \leq 0.9$). Furthermore we require a minimum size of a sub-region of 10^5 km^2. With these criteria, three sub-regions are defined in each region, which results in overall seven distinct sub-regions in JJA and SON and nine distinct sub-regions in DJF and MAM (Fig. 1). For example, **ARM** denotes the sub-region with intermediate sea ice cover in the High Arctic and **NOS** the sub-region with mainly open ocean in the Nordic Seas. In these sub-regions and based on the surface parameters listed above, anomalous and extreme Arctic seasons are defined using a method based on principal component analysis (PCA) as detailed in the following.

2.3 Definition of anomalous and extreme seasons

To determine in an objective way whether a season is anomalous or extreme, a PCA is performed for each sub-region. For that purpose, the seasonal anomalies of the six variables (referred to as precursors) are standardized with their inter-seasonal standard deviation to ensure comparability and equal weighting of the different parameters. Here, the variables H_S, H_L, R_S and R_L, which all contribute to the surface energy balance (E_S), are weighted by the maximum standard deviation of the four E_S components, thus emphasizing variables contributing stronger to E_S variability. We use the PCA to reduce the dimensionality of the six-parameter phase space to two dimensions by focusing on the first and second principal component ($\widetilde{PC1}$ and $\widetilde{PC2}$). $\widetilde{PC1}$ and $\widetilde{PC2}$ maximize the so-called "explained variance", which is the explained proportion of the total inter-seasonal variability in the six-dimensional phase space of the precursors.

To define extreme and anomalous seasons, $\widetilde{PC1}$ and $\widetilde{PC2}$ are first rescaled by their respective standard deviation (σ_1 and σ_2), such that outliers in both PCs are treated similarly independent of the variance explained by $\widetilde{PC1}$ and $\widetilde{PC2}$, thus providing a measure for the unusualness of each season with respect to each of the principal components (from now on, we will refer to these rescaled components as $PC1$ and $PC2$). Then, the Euclidian distance in the reduced phase space spanned by the two rescaled components, the so-called "Mahalanobis distance" (d_M), is calculated as:

$$d_M = \sqrt{PC1^2 + PC2^2} = \sqrt{\frac{\widetilde{PC1}^2}{{\sigma_1}^2} + \frac{\widetilde{PC2}^2}{{\sigma_2}^2}}. \quad (1)$$

This measure d_M can now be used to quantify how strongly a particular season deviates from climatology, representing the combination of the seasonal anomalies of the six variables. We therefore refer to d_M as "anomaly magnitude" of a particular season. Seasons with $d_M \geq 3$ are defined as "extreme seasons", and seasons with $3 > d_M \geq 2$ as "anomalous seasons".

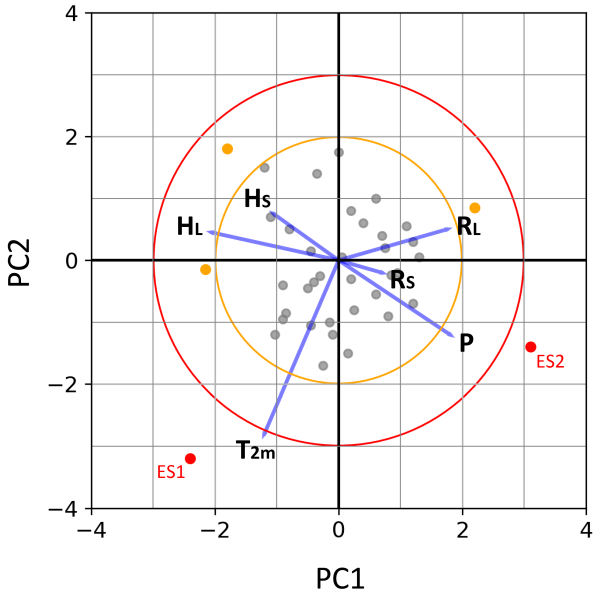

Figure 2. Schematic PCA biplot ~~for a specific region and season~~ with PC1 along the x-axis and PC2 along the y-axis. Grey dots represent single seasons, red (orange) dots show extreme (anomalous) seasons. Blue lines represent the projections of the original parameters onto the first two principal components. Values of d_M=2 and d_M=3 are shown by orange and red circles, respectively.

The phase space of the rescaled principal components can be illustrated using a biplot (Fig. 2), similar as in Graf et al. (2017). The axes of such a plot represent PC1 and PC2, respectively, and each dot represents one season in the study period, whereby anomalous and extreme seasons are shown as colored dots. The closer two dots are, the more similar are the anomalies of the corresponding seasons. Radial vectors show the relative contribution of the precursor variables to PC1 and PC2, whereby the projected values of a vector on both axes illustrates the weight on the respective PC. In the case shown in Fig. 2, the vector for T_{2m} is mainly aligned along PC2, thus T_{2m} variability is important for the second principal mode of variability in the six-dimensional phase space. Relatively longer (shorter) vectors indicate a larger (smaller) contribution of the precursor to the explained variance. If two vectors are approximately perpendicular, the precursors are uncorrelated. This interpretation of correlations is more precise, the higher the explained variance by PC1 and PC2 (Gabriel, 1971, 1972). The relative position of each season in the biplot (i.e., the scores) with respect to the precursor vectors indicates the contribution of the different precursor variables to the anomaly magnitude d_M in the considered season. For instance, seasons with a positive T_{2m} anomaly are positioned in the direction of the T_{2m} vector and seasons with a negative T_{2m} anomaly in the opposite direction.

In the example given in Fig. 2, the variables T_{2m} and P show no correlation, whereas H_S and H_L are positively correlated and H_S and P are strongly anti-correlated. Further, T_{2m} shows the largest contribution to the variance explained by PC1 and

PC2 (mainly determining PC2) whereas H_L, R_S and R_L mostly contribute to PC1. R_S contributes the least to the explained variance. Two seasons with $d_M \geq 3$ are marked as extreme season 1 (ES1) and extreme season 2 (ES2). Their score vectors are roughly orthogonal to each other, which indicates that a different combination of anomalies and thus different processes are decisive for explaining their large anomaly magnitudes. In this example, ES1 is mainly determined by a positive T_{2m} anomaly, while ES2 is an anomalously wet season with negative surface heat flux anomalies, as the respective precursor vectors are directed more or less directly towards (P) respectively away (H_L, H_S) from ES2.

3 Spatial and temporal variability of Arctic seasons

In order to characterize Arctic seasons in general, we first analyze the ~~regional and temporal variability~~ co-variability of seasonal-mean anomalies of surface temperature ($\overline{T_{2m}{}^*}$), precipitation ($\overline{P^*}$) and surface energy balance ($\overline{E_S{}^*}$) in the three regions, considering the varying surface conditions of the different sub-regions (Fig. 3). We are interested in correlations between the seasonal anomalies, how their magnitudes vary between the regions, and in aspects of the seasonal substructure (e.g., is an anomalously warm season constantly warm?).

In winter, warm seasons are generally wetter and cold seasons are drier (Fig. 3~~a). $\overline{E_S{}^*}$ and $\overline{T_{2m}{}^*}$ are positively correlated, thus warm winters show in general a positive $\overline{E_S{}^*}$ and vice versa for cold winters, whereby for the relationship between $\overline{E_S{}^*}$ and $\overline{P^*}$ a strong dependency on the respective surface type can be observed.~~ a-c), except for sub-regions **NOS** and **KBS** (see also Table S1 in the supplement). In regions with $\mathrm{SIC}_{\mathrm{clim}} > 0.9$ (Fig. 3a), $\overline{T_{2m}{}^*}$ and $\overline{P^*}$ are strongly positively correlated, thus warm winters are almost always (in 79.8 % of the cases) wet and tend to have a positive E_S anomaly (and again vice versa for cold winters). In contrast, regions with $\mathrm{SIC}_{\mathrm{clim}} < 0.1$ in the Nordic ~~and Kara-Barents~~ Seas and Kara and Barents Seas do either show ~~no or~~ only a weak positive or even a slightly negative correlation between $\overline{T_{2m}{}^*}$ and $\overline{P^*}$ ~~.~~ (Fig. 3c). Over the open ocean, warm and dry winters show strongly positive, and cold and wet winters negative $\overline{E_S{}^*}$ values. Regions with intermediate sea ice extent (Fig. 3b) do not show this correlation between ~~$\overline{T_{2m}{}^*}$~~ $\overline{T_{2m}{}^*}$ and $\overline{E_S{}^*}$, but warm winters tend to be wet and cold winters dry, similar to the **ice** sub-regions.

In summer, no correlation between $\overline{T_{2m}{}^*}$ and $\overline{P^*}$ is found, but ~~warm summers usually~~ 73.3 % of the warm summers show a positive $\overline{E_S{}^*}$ and 72.5 % of the cold summers a negative $\overline{E_S{}^*}$, independent of the surface conditions (Fig. 3~~b~~d-f and supplementary Table S2). Regional differences are much smaller during summer, indicating more homogeneous conditions among the sub-regions.

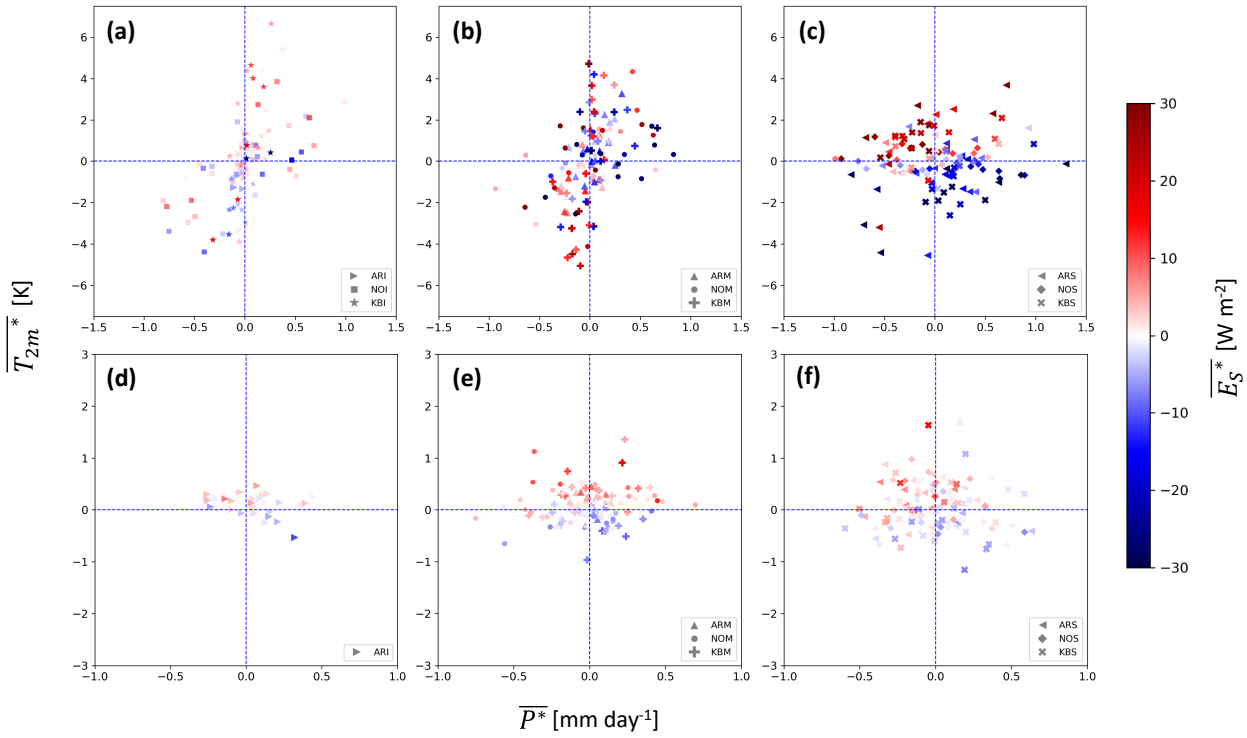

Figure 3. Seasonal-mean anomalies of P ($\overline{P^*}$; mm day^{-1}, along x-axis), T_{2m} ($\overline{T_{2m}}^*$; K, along y-axis) and E_S ($\overline{E_S}^*$; W m^{-2}, color) for 39 seasons ~~and **(a)** 9 sub-regions~~ in **(a-c)** DJF and ~~**(b)** 7~~ **(d-f)** JJA for sub-regions with **(a, d)** SIC$_{\text{clim}} > 0.9$, **(b, e)** $0.1 \leq$ SIC$_{\text{clim}} \leq 0.9$ and **(c, f)** SIC$_{\text{clim}} < 0.1$. Tables S1 and S2 in ~~JJA~~the supplement show correlations and respective p-values for the described relations between the different parameters in each sub-region.

~~Figure 4 shows the~~ In addition to the previously discussed seasonal-mean ~~absolute anomalies~~ ~~$|\overline{T_{2m}}^*|$~~ anomalies, the intra-seasonal variability of the individual parameters is an important and complementary characteristic of Arctic seasons. As we will show in the following, the strength of the intra-seasonal variability can depend, in particular, on the surface conditions. To compare the intra-seasonal variability of $\overline{T_{2m}}^*$, $\overline{P^*}$ and $\overline{E_S}^*$, we consider in Fig. 4 seasonal-mean absolute anomalies $|\overline{T_{2m}}^*|$, $|\overline{P^*}|$ and $|\overline{E_S}^*|$, which are defined as the seasonal mean of the absolute daily anomalies. They are used as a measure for the overall variability of the individual parameters throughout a season. Distinct clusters occur for the different sub-regions in winter (Fig. 4a). Regions in high latitudes and mostly over sea ice such as **ARI** and **ARM** show only small variations in all three variables implying a relatively small amplitude of day-to-day and inter-seasonal fluctuations. In the ~~Kara-Barents~~ Kara and Barents Seas, sub-regions **KBI** and **KBM** show high variability in daily and seasonal T_{2m} and E_S anomalies but a similarly small $|\overline{P^*}|$. In the Nordic Seas, T_{2m} and P are much more variable, except over the open ocean, where T_{2m} anomalies are typically smaller and less variable. P and especially E_S variability is strongly enhanced over the open ocean due to intensified air-sea interaction. The clear distinction of the seasonal-mean absolute anomalies between the different sub-regions reveals

the spatial inhomogeneity of Arctic meteorological conditions in winter, which is due to varying surface conditions as well as differences in seasonal variability between distinct Arctic Seas. This also serves as an a posteriori confirmation of our approach to separately consider Arctic extreme seasons in these sub-regions.

In summer, the variability of the three analyzed parameters is smaller due to reduced meridional gradients of surface temperature and radiation causing smaller T_{2m} and E_S fluctuations (Fig. 4b). Similar to winter, a large variability of T_{2m} occurs in the ~~Kara-Barents~~ Kara and Barents Seas and of P in the Nordic Seas. However, as the surface conditions between the sub-regions become more homogeneous, the regions do not appear in distinct clusters as for winter with the exception of the sub-regions **ARI** and **ARM**, which cover most of the perennial sea ice and show, as in winter, only a small variability of the three parameters. It is further noteworthy that ~~$|\overline{T_{2m}{}^*}|$~~ $|\overline{T_{2m}{}^*}|$ and $|\overline{P^*}|$ are positively correlated, indicating higher variability in P in seasons with larger T_{2m} fluctuations.

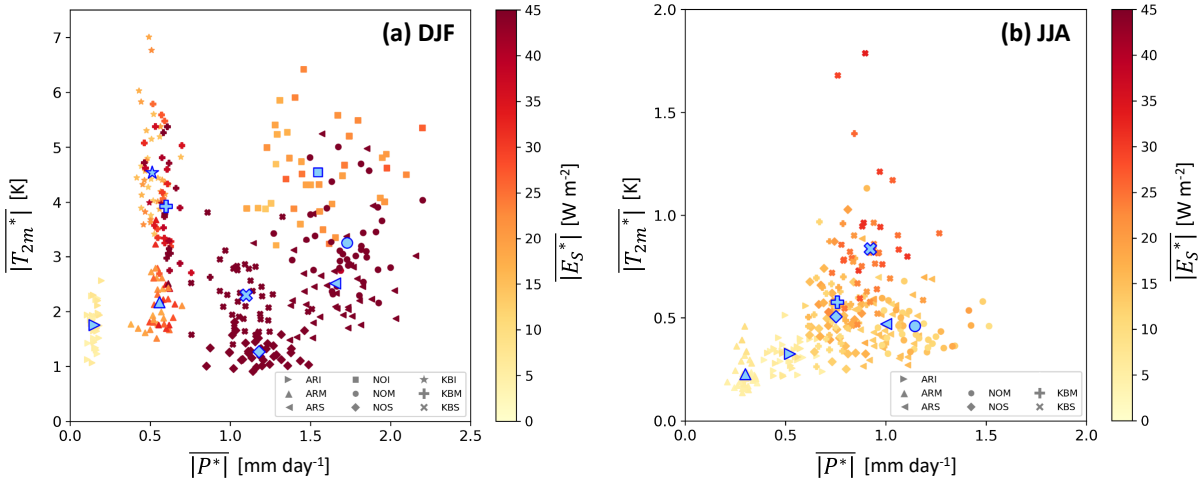

Figure 4. Seasonal-mean absolute anomalies of P ($|\overline{P^*}|$; mm day^{-1}, along x-axis), T_{2m} ($|\overline{T_{2m}{}^*}|$; K, along y-axis) and E_S ($|\overline{E_S{}^*}|$; W m^{-2}, color) for 39 seasons and **(a)** 9 sub-regions in DJF and **(b)** 7 sub-regions in JJA. Blue symbols mark average values for each sub-region.

To better understand the seasonal substructure of Arctic winters and summers, we compare the seasonal-mean anomalies with the seasonal-mean absolute anomalies for T_{2m}, P and E_S in selected sub-regions in DJF (Fig. 5) and JJA (Fig. 6; for remaining sub-regions see supplementary Figs. S2 and S3). The ratio of seasonal-mean and seasonal-mean absolute anomalies, $\frac{\overline{x^*}}{|\overline{x^*}|}$, is indicative for the temporal persistency of an anomaly throughout a season~~, thus~~. Thus, the location of a season in the di-

agrams provides information about the substructure of the season in terms of the considered parameter. ~~For instance~~In general, the further to the right, the more positive is the seasonal-mean anomaly of the shown parameter ~~,~~ and the further to the ~~top, the larger is the seasonal-mean absolute anomaly. If~~ left, the more negative. The closer the seasonal-mean anomaly is ~~close~~ to the seasonal-mean absolute anomaly (dots ~~along the grey line~~close to the outer stippled grey line representing $\frac{\overline{\chi^*}}{|\overline{\chi^*}|} = \pm 1$), the more persistent ~~is the anomaly during the season~~the anomaly is throughout the season. Thus, we define seasons with $0.8 < \frac{\overline{\chi^*}}{|\overline{\chi^*}|} < 1$ as seasons with a "continuous" anomaly. With a decreasing value of $\frac{\overline{\chi^*}}{|\overline{\chi^*}|}$, the seasons are located further away from the outer stippled grey lines, meaning that positive or negative anomalies in the respective parameter occur more episodically throughout the season. The closer a season is positioned towards the blue dashed line where $\overline{\chi^*} = 0$ and thus $\frac{\overline{\chi^*}}{|\overline{\chi^*}|} = 0$, the more positive and negative daily anomalies cancel each other, leading to a weak overall seasonal anomaly. The value of $|\overline{\chi^*}|$ is further indicative of the magnitude of the daily anomalies throughout a season. A season located at the top of the plot shows stronger daily anomalies than a season with the same $\frac{\overline{\chi^*}}{|\overline{\chi^*}|}$ ratio but a smaller $|\overline{\chi^*}|$.

For example, a season can be anomalously warm, because the daily-mean T_{2m} values are ~~continuously~~ larger than the climatology on almost all days of the season, resulting in $|\overline{T_{2m}{}^*}| \frac{\overline{T_{2m}{}^*}}{|\overline{T_{2m}{}^*}|} \approx 1$. With a decreasing ratio of the anomaly metrics, e.g., $\frac{\overline{T_{2m}{}^*}}{|\overline{T_{2m}{}^*}|} = \overline{T_{2m}{}^*}$~~.In contrast, if $|\overline{T_{2m}{}^*}| > \overline{T_{2m}{}^*} > 0$, the anomalously warm season~~ 0.5, the season is still anomalously warm, but it results from several warm episodes alternating with weaker and/or shorter periods with negative ${T_{2m}}^*$ values. If ~~the seasonal-mean absolute anomaly is much larger compared to the seasonal-mean anomaly, i.e., $|\overline{T_{2m}{}^*}| \frac{\overline{T_{2m}{}^*}}{|\overline{T_{2m}{}^*}|} \approx \gg \overline{T_{2m}{}^*}$, then the variability of T_{2m} is large with several intense warm and cold episodes, which~~ 0, cold and warm episodes cancel each other ~~out~~ leading to a weak overall seasonal anomaly. Comparing seasons with the same $\frac{\overline{T_{2m}{}^*}}{|\overline{T_{2m}{}^*}|}$, the ones positioned further along the y-axis (showing larger values of $\overline{T_{2m}{}^*}$ and $|\overline{T_{2m}{}^*}|$) show a larger variability in T_{2m} with more intense warm and/or cold episodes.

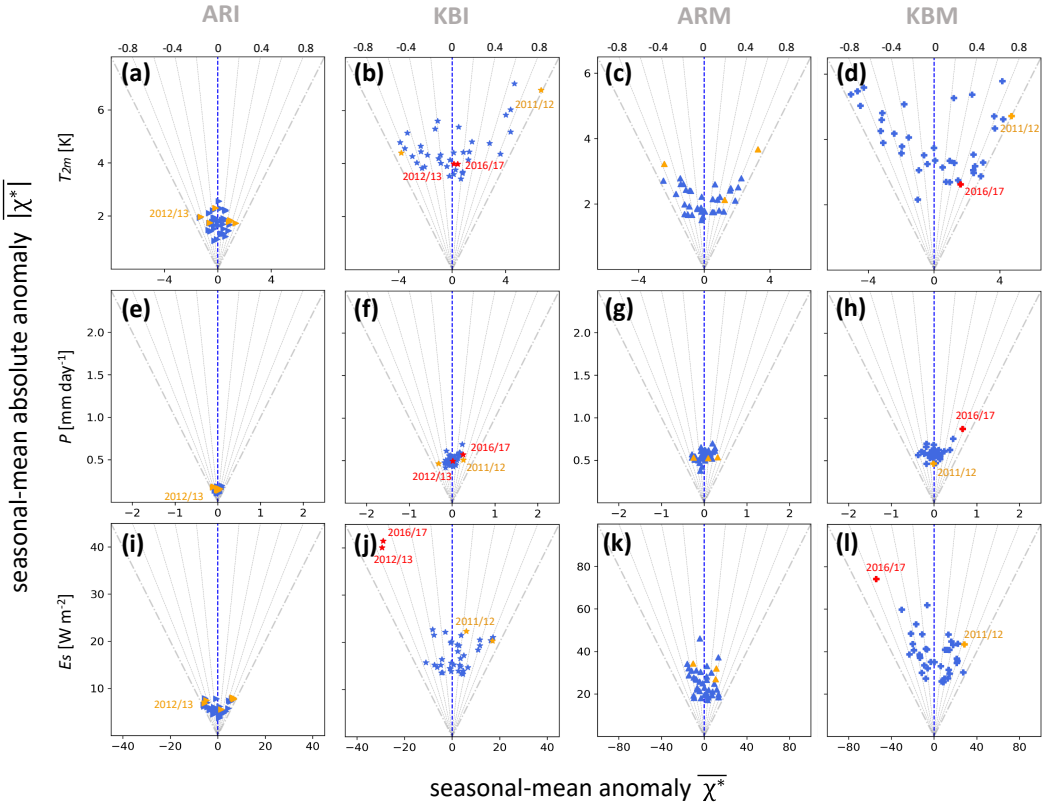

Figure 5. Seasonal-mean anomalies ($\overline{\chi^*}$, along x-axis) vs. seasonal-mean absolute anomalies ($|\overline{\chi^*}|$, along y-axis) in DJF for **(a-d)** T_{2m} (K), **(e-h)** P (mm day^{-1}), and **(i-l)** E_S (W m^{-2}) in sub-regions **ARI**, **KBI**, **ARM** and **KBM**. The ratio of both measures, $\frac{\overline{\chi^*}}{|\overline{\chi^*}|}$, is additionally visualized by grey dashed lines. $\frac{\overline{\chi^*}}{|\overline{\chi^*}|} = \pm 1$ is shown by stippled grey lines and $\frac{\overline{\chi^*}}{|\overline{\chi^*}|} = 0$ is shown by a dashed blue line. Red (orange) markers represent extreme (anomalous) seasons (see Sect. 2.3) and selected case study seasons are labeled. ~~The stippled grey line marks where the seasonal-mean anomaly equals the seasonal-mean absolute anomaly~~Remaining sub-regions are shown in supplementary Fig. S2.

The seasonal substructures of the three parameters differ. In particular during summer, several seasons show continuous ${T_{2m}}^*$ (Fig. 6a-d) and/or almost continuous ${E_S}^*$ values (Fig. 6i-l), including several clear outlier seasons in terms of $\overline{{T_{2m}}^*}$ (Fig. 6a, c, d). In winter, the overall T_{2m} variability is much larger and only very few seasons show distinct $\overline{{T_{2m}}^*}$ outliers (Fig. 5a-d). Further, no continuous P^* can be observed (Figs. 5e-h and 6e-h), indicating that also in very wet seasons precipitation is episodic and includes dry periods. In addition, and maybe less evident, also the driest seasons feature some precipitation events.

The influence of the different surface conditions becomes apparent in particular for the seasonal substructure of E_S anomalies. In regions with intermediate or high $\mathrm{SIC}_{\mathrm{clim}}$, where surface heat fluxes are small and E_S is mainly determined by net

surface radiation, seasonal anomalies can continuously have the same sign, especially in summer, as shown by points near the diagonal in Fig. 6i and j. Over the open ocean, where surface heat fluxes are much more important, daily-mean E_S values fluctuate significantly around the climatology, which results in a large $\overline{|E_S{}^*|}$ but only a small $\overline{E_S{}^*}$ (Fig. 6l).

In **KBM** and **KBS**, a different distribution of E_S anomalies occurs in DJF and JJA. Winters with a negative $\overline{E_S{}^*}$, which is often caused by several episodes of cold air outbreaks (Papritz and Spengler, 2017), tend to show enhanced E_S variability throughout the season (Fig. 5l) compared to winters with a positive $\overline{E_S{}^*}$, where CAOs are less frequent. The opposite occurs in summer, when periods of increased net surface radiation can cause a positive $\overline{E_S{}^*}$ and enhanced $\overline{|E_S{}^*|}$ compared to seasons with a negative $\overline{E_S{}^*}$ (Fig. 6k and l).

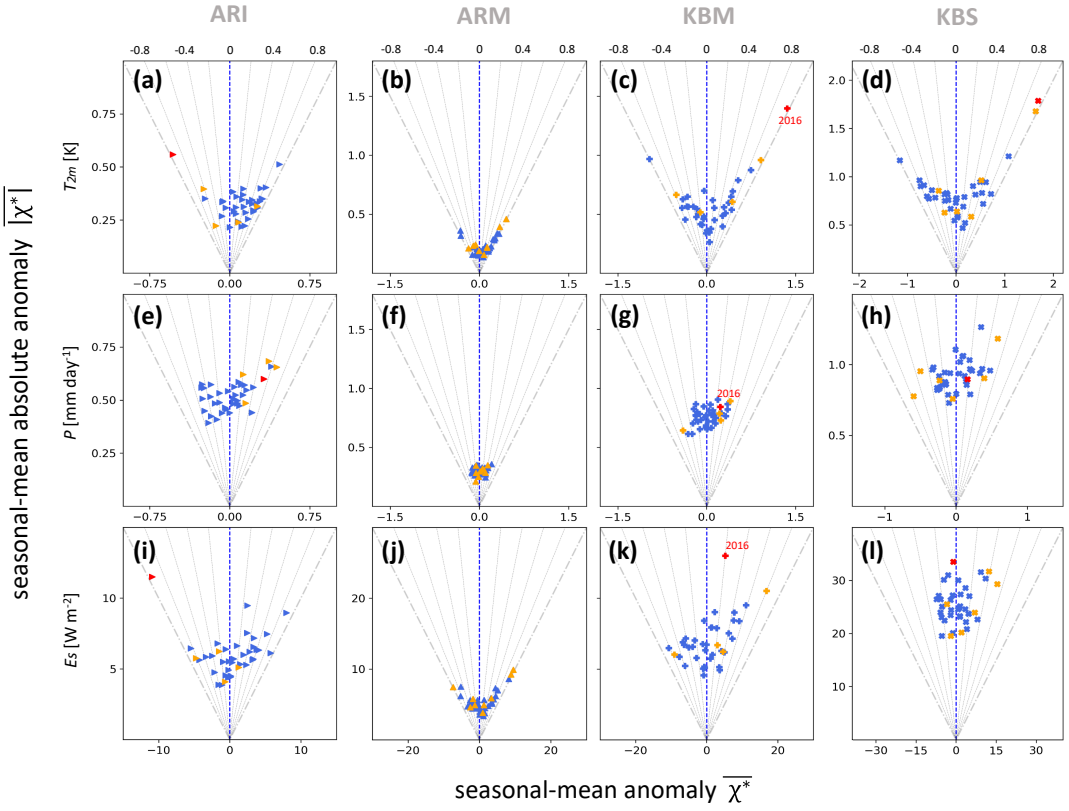

Figure 6. Same as Fig. 5 but for JJA in sub-regions **ARI**, **ARM**, **KBM** and **KBS**. The extreme summer 2016 is labeled in **(c, g, k)** due to its role in the preconditioning of the extreme winter 2016/17 (see subsection 5.2). Remaining sub-regions are shown in supplementary Fig. S3.

4 PCA results

In the previous section, we discussed the co-variability of T_{2m}, P and E_S and regional differences for Arctic winter and summer seasons as well as the seasonal substructure of these parameters. In a next step, we identify and then characterize anomalous Arctic seasons, based on the combination of the seasonal-mean anomalies of the three surface parameters~~discussed above~~. To this end, a PCA is performed for each season (DJF, MAM, JJA, SON) and sub-region, as explained in Sect. 2.3. Figures 7 and 8 show the resulting biplots for DJF and JJA (for MAM and SON see Figs. ~~S2 and S3~~ S5 and S6 in the supplementary material). Depending on the region and sub-region, the contributions of the precursor variables to the principal components PC1 and PC2 vary, which usually explain about ~~80 – 90%~~ 80% – 90% of the total variance in the combined seasonal anomalies. Further we can show that, following the method introduced in North et al. (1982), the first two PCs in DJF and JJA are, with exception of sub-region **ARM** in JJA, always statistically distinguishable from the others (see supplementary Fig. S4). This implies that by considering PC1 and PC2, we capture most of the variance.

In winter, sub-regions over ice show a positive correlation between $\overline{T_{2m}}^*$ and $\overline{P}^*$ (Fig. 7a, d, g). This correlation is particularly strong in the High Arctic, where precipitation events during winter are predominantly caused by synoptic weather systems that transport warm and moist air masses into the region ~~(e.g. Webster et al., 2019; Papritz and Dunn-Sigouin, 2020)~~(e.g., Webster et al., 2019; I $\overline{T_{2m}}^*$, $\overline{P}^*$ and $\overline{R_L}^*$ mainly determine PC1 and thus the direction of maximum variance in the phase space spanned by all precursor variables in **ice** sub-regions. Surface sensible and latent heat flux anomalies are positively correlated and mostly uncorrelated with $\overline{T_{2m}}^*$ and $\overline{P}^*$ as they contribute mostly to PC2.

Similarly, sub-regions with intermediate sea ice concentration show a positive correlation of $\overline{T_{2m}}^*$ and $\overline{P}^*$ (Fig. 7b, e, h), although slightly weaker than over ice for regions **KB** and **NO**. Again, the heat fluxes are mostly uncorrelated with $\overline{T_{2m}}^*$ and slightly negatively correlated with $\overline{P}^*$, particularly $\overline{H_L}^*$. $\overline{R_L}^*$ is contributing less to the variance in **mixed** regions, which indicates a comparatively lower importance of radiation compared to heat fluxes for determining the seasonal variability.

Over the open ocean (Fig. 7c, f, i), a positive correlation between the heat flux anomalies and $\overline{T_{2m}}^*$ can be observed, indicating increased surface fluxes from the ocean into the atmosphere during periods with anomalously cold temperatures. Unlike over ice, the maximum variance over open water is mainly determined by the surface heat fluxes. $\overline{P}^*$ is mostly uncorrelated to the other variables and strongly related to PC2, reflecting that precipitation can occur in warm conditions (e.g., warm sector of a cyclone) and in cold conditions (CAO).

Arctic summer seasonal variability is mainly determined by $\overline{T_{2m}}^*$, $\overline{P}^*$ and $\overline{R_S}^*$, whereby $\overline{T_{2m}}^*$ and $\overline{P}^*$ are mostly uncorrelated in all regions (Fig. 8). Whereas $\overline{T_{2m}}^*$ shows only weak correlations with other parameters in general, $\overline{P}^*$ is strongly anti-correlated with $\overline{R_S}^*$ in sub-regions **NOS** and **ARS** (Fig. 8f and i), most likely due to the presence of clouds during precipitation events. In sub-regions **ARI** and **ARM** (Fig. 8g and h), $\overline{R_L}^*$ additionally influences the seasonal variability and strongly

correlates with $\overline{T_{2m}{}^*}$, again emphasizing the importance of clouds in this region.

Season	Sub-regions	d_M	$\overline{T_{2m}{}^*}$ [K]	$\overline{P^*}$ [mm day^{-1}]	$\overline{E_S{}^*}$ [W m^{-2}]	Area [10^5 km^2]
DJF 2004/05	ARS	3.2	–0.13 *(–0.07)* [21–]	+1.30 *(+2.73)* **[1+]**	–47.10 *(–2.00)* **[1–]**	3.5
DJF 2012/13	KBI	3.0	+0.13 *(+0.05)* [18+]	+0.02 *(+0.12)* [19+]	–29.48 *(–3.07)* **[1–]**	~~5.3~~5.4
DJF 2016/17	KBI	3.4	+0.41 *(+0.16)* [16+]	+0.25 *(+1.96)* [2+]	–29.00 *(–3.02)* [2–]	~~22.8~~5.4
	KBM	3.3	+1.61 *(+0.59)* [13+]	+0.67 *(+3.44)* **[1+]**	–54.20 *(–3.03)* **[1–]**	10.7
	KBS	3.1	+0.83 *(+0.65)* [14+]	+0.98 *(+3.03)* **[1+]**	–19.14 *(–0.81)* [8–]	6.8
JJA 2013	ARI	3.2	–0.53 *(–2.90)* **[1–]**	+0.32 *(+1.75)* [4+]	–10.9 *(–3.21)* **[1–]**	14.3
JJA 2016	KBM	3.1	+1.36 *(+3.27)* **[1+]**	+0.23 *(+1.18)* [7+]	+0.52 *(+0.91)* [8+]	~~16.7~~11.6
	NOM	3.3	+1.13 *(+3.47)* **[1+]**	–0.37 *(–1.10)* [8–]	+9.27 *(+1.65)* [4+]	5.1
MAM 1990[1]	NOI	3.7	+0.37 *(+0.27)* [17+]	–0.16 *(–0.37)* [16–]	–1.51 *(–0.47)* [12–]	~~82.2~~1.3
	ARI	4.1	+3.08 *(+3.45)* **[1+]**	+0.25 *(+3.81)* **[1+]**	+2.36 *(+1.23)* [4+]	80.9
MAM 1996	NOM	3.3	+1.32 *(+1.20)* [6+]	–0.54 *(–1.25)* [4–]	+33.96 *(+2.69)* **[1+]**	5.8
SON 1995	KBM	3.0	+0.68 *(+0.42)* [16+]	–0.06 *(–0.27)* [15–]	–27.11 *(–2.99)* **[1–]**	10.7
SON 2007	ARM	3.3	+1.33 *(+1.40)* [8+]	+0.06 *(+0.78)* [11+]	–15.2 *(–3.47)* **[1–]**	52.7
SON 2018	ARI	3.2	+1.63 *(+1.36)* [4+]	+0.31 *(+3.07)* **[1+]**	–2.76 *(–1.60)* [4–]	32.3

Table 2. Extreme seasons in DJF, JJA, MAM and SON, including the affected sub-regions and respective Mahalanobis distance (d_M, see Sect. 2.3), the seasonal-mean anomalies of T_{2m}, P and E_S (standardized seasonal-mean anomalies in ~~brackets~~parentheses) and ~~total~~ affected area per sub-region. The rank of each seasonal-mean anomaly with respect to all seasons is given in brackets, with "1+" denoting rank 1 in terms of a positive anomaly (e.g., wettest season) and "1–" denoting rank 1 in terms of a negative anomaly (e.g., driest season).

4.1 Arctic extreme and anomalous seasons

~~Using~~ As explained in Sect. 2.3, by using a threshold for the anomaly magnitude ($d_M \geq 3$~~, see Sect. 2.3~~), seasons that appear as clear outliers in their respective PCA biplot are defined as extreme seasons, whereas seasons located at the edges of the point cloud formed by all seasons are characterized as anomalous seasons ($3 > d_M \geq 2$). The two thresholds are chosen

[1] Extreme season MAM 1990 in sub-region **NOI** shows rank **[1+]** for R_S, rank [7+] for H_S, rank [9–] for H_L and rank **[1–]** for R_L. Although single components of E_S show rank 1, but in opposite directions, this leads to an overall medium rank [12–] for E_S.

pragmatically to distinguish seasons with different anomaly magnitudes and to classify the season with the largest anomaly magnitude as “extreme season". ~~The term extreme season is appropriate as their return period corresponds to approximately 40 years in a given region. With our~~ Using these thresholds we find 2 extreme seasons in DJF, JJA and MAM, respectively, and 3 extreme seasons in SON (Table 2). With this total number of extreme seasons, the return period of such a season corresponds to approximately 40 years, which has been used as an adequate measure for defining extreme seasons by several studies, e.g., Röthlisberger et al. (2021). The number of sub-regions where one particular season is identified as extreme varies between one and three, however the varying size of the sub-regions and thus significant differences in the extent of the affected area have to be considered. Further we identify on average 3.3 anomalous seasons per sub-region in DJF, 5 anomalous seasons per sub-region in JJA, 4.7 anomalous seasons per sub-region in MAM and 4.4 anomalous seasons per sub-region in SON (see supplementary Tables ~~S1-S4~~S3-S6).

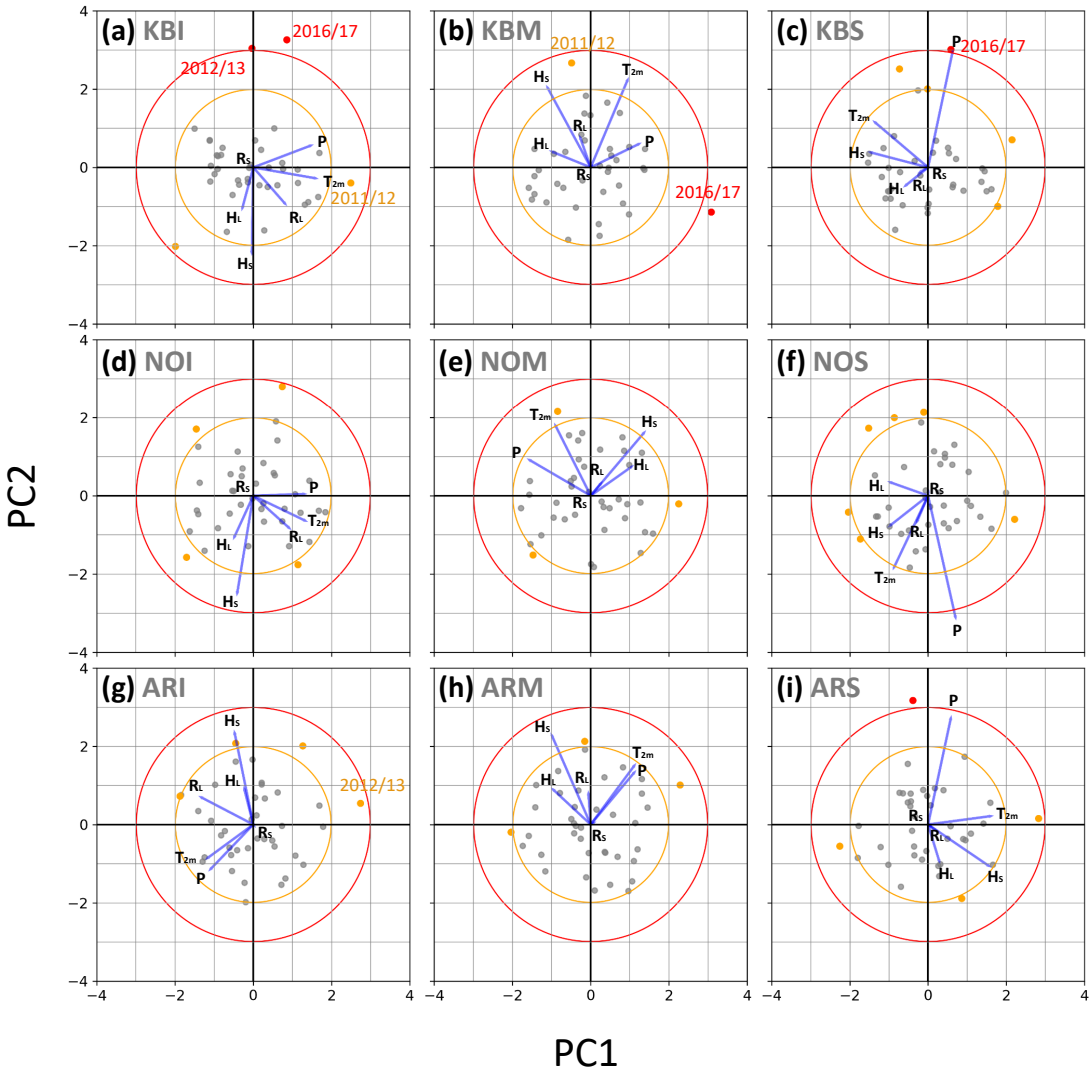

Figure 7. PCA biplot for all sub-regions in DJF with PC1 and PC2 along the x- and y-axis, respectively. Every season is represented by a grey dot, red and orange dots show extreme and anomalous seasons, respectively. Blue lines represent the coefficients of the precursor variables. Red and orange circles represent d_M=3 and d_M=2, the thresholds used for extreme and anomalous seasons, respectively. Selected case study seasons are labeled.

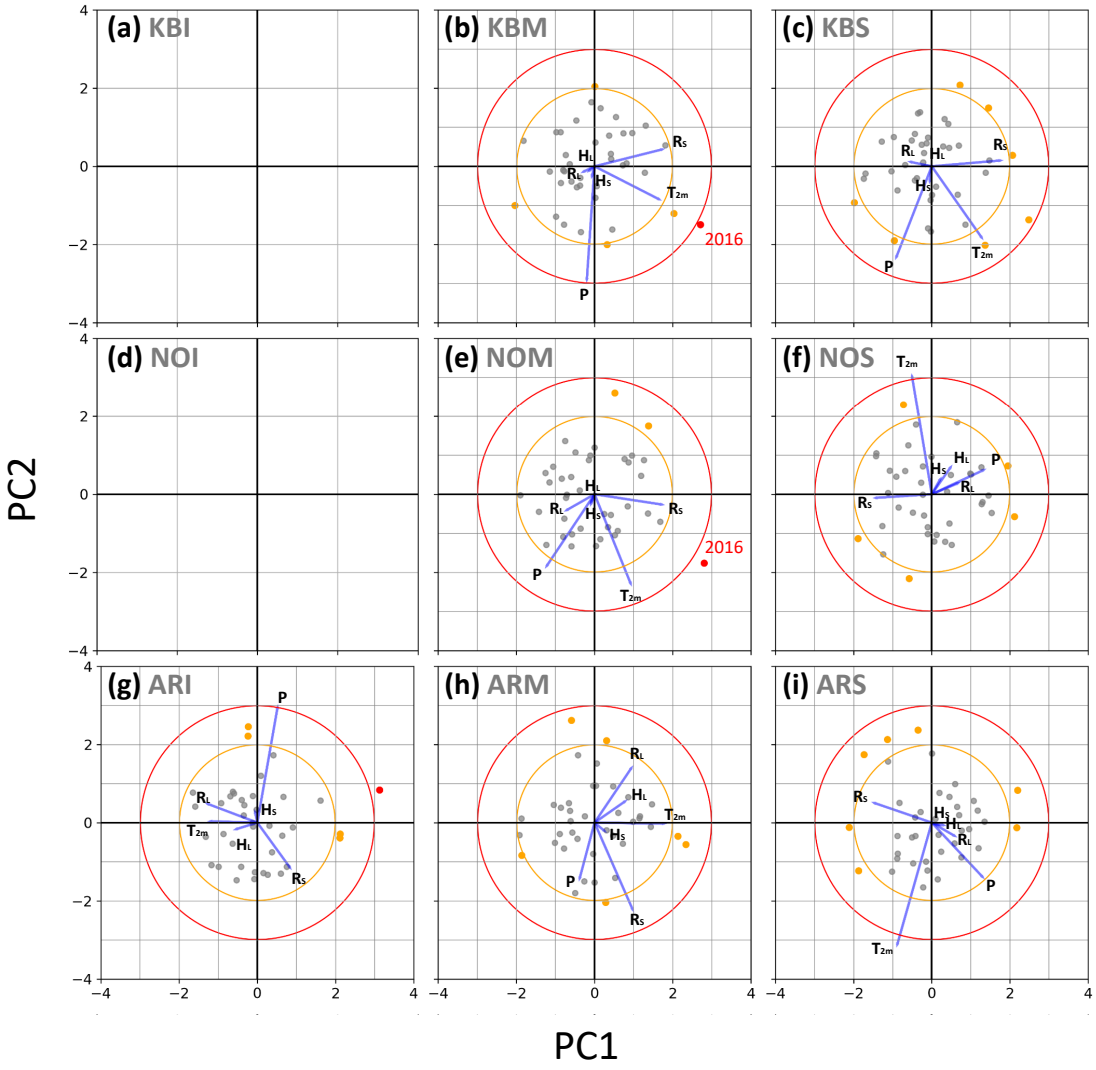

Figure 8. As Fig. 7 but for JJA. No biplots are shown for the sub-regions **KBI** and **NOI**, because they fall below the minimum size threshold of 10^5 km^2 in summer. The extreme summer 2016 is labeled in **(b, e)** due to its role in the preconditioning of the extreme winter 2016/17 (see subsection 5.2).

~~It is now interesting to~~ After identifying Arctic extreme and anomalous seasons as well as the surface parameters determining their variability in the different sub-regions, we are now interested in the substructure of such seasons with respect to T_{2m}, P and E_S. Therefore, we briefly reconsider Figs. 5 and 6 and focus on the extreme and anomalous seasons, shown by red and orange dots, respectively, in comparison to all seasons in the study period. By design, extreme seasons with $d_M \geq 3$ have very large anomalies for at least one parameter (see ranks for seasonal-mean anomalies in Table 2), for example the strong

positive and nearly continuous $\overline{P^*}$ in the extreme winter in **KBM** (Fig. 5h) or the negative $\overline{E_S{}^*}$ in both extreme winters in **KBI** (Fig. 5j). In summer, all extreme seasons are characterized by a strong $\overline{T_{2m}{}^*}$ outlier (Fig. 6a, c, d), which coincides with an equally strong $\overline{E_S{}^*}$ outlier in **ARI** (Fig. 6i). Similarly, most anomalous seasons also show outliers or anomalies near the edge of the point cloud for at least one parameter. However, some anomalous seasons don't show very strong anomalies in one particular parameter, which implies that for these seasons it is the combination of several parameters that makes them anomalous. In a given region, several extreme or anomalous seasons can have similar seasonal anomalies, for instance both extreme winters in **KBI** (Fig. 5b, f, j) and two anomalous and one extreme summers in **ARI** (Fig. 6a, e, i), indicating similar characteristics and most likely also underlying processes causing the anomalous nature of these seasons. However, in other regions with multiple anomalous seasons, they show a similar behavior in one but a contrasting behavior in another variable. For example, the anomalous winters in **KBM** both have a positive $\overline{T_{2m}{}^*}$ but different signs in their respective $\overline{E_S{}^*}$ (Fig. 5d and l). We thus expect different processes to be responsible for these seasons to be anomalous.

Based on the results of the PCA analysis and Fig. 5, ~~two extreme and one anomalous winters~~ the following winter seasons are chosen for detailed case studies to better understand their seasonal substructure as well as the underlying processes~~. The selected seasons are the~~ : The winters 2011/12 and 2016/17 in the ~~Kara-Barents~~ Kara and Barents Seas and the winter 2012/13 in **ARI**. ~~A third~~ We do not consider the extreme winter in ~~region~~ **ARS** ~~is disregarded~~in 2004/05, as **ARS** is only a very small region that consists of two remote fragments and thus the meaningful analysis of the involved processes would be less straightforward. Furthermore this selection allows to, on one hand, contrast two seasons in the same geographical region, and on the other hand also point out differences in terms of the underlying processes in a region at the edge of the Arctic and in the High Arctic. This choice of case study seasons is subjective and motivated by the intention to reveal the diversity and complexity of the involved processes. It is further strongly limited by the available amount of suitable seasons for in-depth investigation. Choosing two winter seasons in the same region allows us to emphasize inter-annual variability, while avoiding additional effects of seasonal variations.

5 Case Studies

5.1 DJF 2011/12

The winter of 2011/12 is classified as an anomalous season in **KBI** and **KBM**. In both sub-regions, this winter shows the largest positive $\overline{T_{2m}{}^*}$ during the 39-year study period (Fig. 7b and d). The time series in Fig. 9a shows that the daily-mean surface temperature is continuously above the climatology (consistent with the fact that the dots in Fig. 5b and d are on the diagonal). In **KBI**, $\overline{T_{2m}{}^*}$ is the main contributor to this season's anomaly magnitude, supported by positive $\overline{P^*}$ and $\overline{R_L{}^*}$ (Figs. 5b and f, and 7a). In **KBM**, positive $\overline{T_{2m}{}^*}$ and $\overline{H_S{}^*}$ mainly determine the exceptional character of this winter (Figs. 5d and 7b), which also leads to one of the most positive $\overline{E_S{}^*}$ compared to all winters in the study period (Fig. 5l).

In DJF 2011/12, $\overline{{T_{2m}}^*}$ is about +6.6 K in **KBI** and +4.7 K in **KBM**. In the whole region, during December, values are continuously around +6 K above climatology, before approaching more ~~normal~~ average levels at the beginning of January (Fig. 9a). The largest ${T_{2m}}^*$ values are reached in February. The SIC anomaly shows an opposite behavior and is continuously negative, reaching values close to climatology only at the beginning of the season and during the period with reduced ${T_{2m}}^*$ in January (Fig. 9c). Similarly to the other variables, we here calculate the SIC anomaly using a transient climatology, as this effectively removes non-linear SIC trends in the ~~Kara-Barents~~ Kara and Barents Seas (see Fig. S1c and d in the supplement). Daily-mean E_S values are strongly correlated with daily-mean T_{2m}, resulting in mostly positive ${E_S}^*$ during the particularly warm episodes and shorter periods of negative ${E_S}^*$ when ${T_{2m}}^*$ is reduced (Fig. 9b). The positive $\overline{{E_S}^*}$ is mainly due to a strongly positive $\overline{{H_S}^*}$, i.e., strongly reduced heat fluxes into the atmosphere, favored by the warm surface temperatures and comparatively few CAOs (see next paragraph). During the period with the largest ${T_{2m}}^*$ in February, when the surface air temperatures exceed 0 °C at several grid points on multiple days, even positive H_S values occur over the open ocean (not shown). Daily P values show only small deviations from climatology, except for the first five days of the season and in the beginning of February (Fig. 9d).

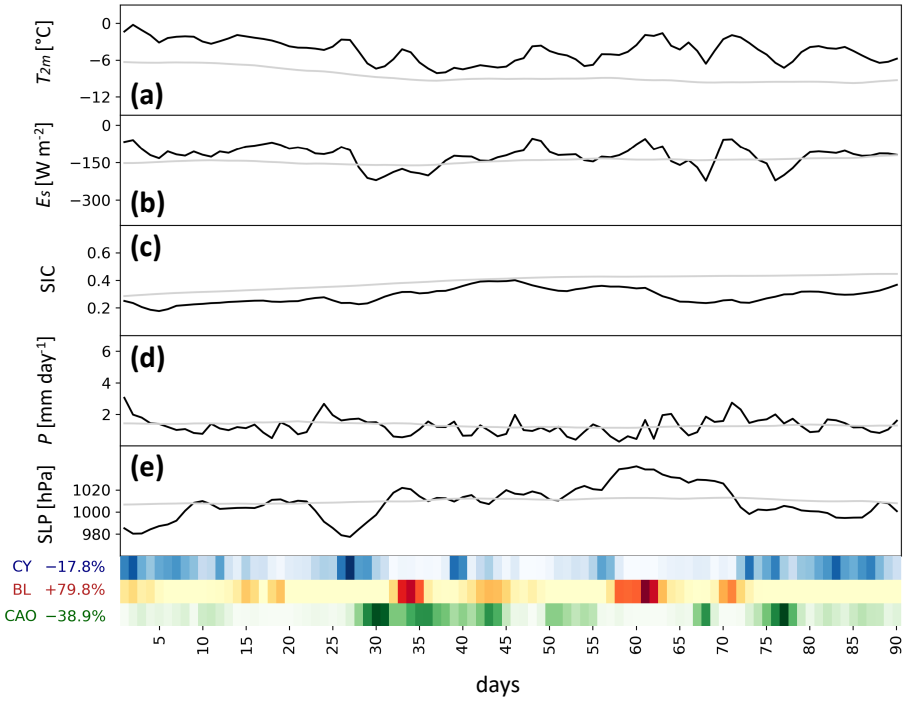

Figure 9. Time series of daily-mean **(a)** T_{2m} (in °C), **(b)** E_S (in W m^{-2}), **(c)** SIC~~and ,~~ **(d)** P (in mm day^{-1}) and **(e)** sea-level pressure (SLP, in hPa) averaged in the region of the ~~Kara-Barents~~ Kara and Barents Seas (**KBI**, **KBM**, and **KBS**) in DJF 2011/12 (black lines). The transient climatology is shown by grey lines. Blue, orange, and green heatmaps at the bottom of the figure show the daily-mean coverage of the region by cyclones, blocks, and CAOs, respectively (the darker the color the higher the coverage). Relative frequency anomalies of the three weather systems are given in percentages. The horizontal axis indicates days since the start of the season with day 1 corresponding to 01 December.

It is now interesting to compare the time series of the basic variables with the occurrence of specific weather systems. The colored heatmaps at the bottom of Fig. 9 provide information about the occurrence of cyclones, blocks and CAOs in the ~~Kara-Barents Seas.~~ Kara and Barents Seas. As each weather system is identified as an object described by a two-dimensional binary field (grid points that belong to a system have a value of 1 and other grid points have a value of 0), the weather system frequency field is calculated by time averaging of these binary fields. For example, if a cyclone mask covers a grid point at 25 % of all times, then time averaging of the binary fields yields 0.25, corresponding to a cyclone frequency of 25 %. Here, the color intensity is representative for the daily mean weather system frequency averaged over the area of the sub-region, thus it indicates the percentage of the sub-regions' area ~~which~~ that overlaps with a cyclone, blocking or CAO mask on a daily basis. The repeated passage of cyclones (Fig. 9, blue heatmap) originating from the Nordic Seas (not shown) ensures the continuous transport of warm and moist air masses into the ~~Kara-Barents~~ Kara and Barents Seas throughout several periods, mostly during December and February. Yet, in the wintertime average, cyclone frequency in this region was slightly below climatology (as

further discussed in section 5.3). In contrast, CAO frequency (Fig. 9, green heatmap) was strongly reduced while blocking frequency was substantially increased (Fig. 9, red heatmap) in this season. CAOs, which often occur after the passage of a cyclone in the cyclones' cold sector, as can be seen for example around days 30, 43 and 77, usually lead to a strong decrease in T_{2m} and E_S (associated with intense surface fluxes). Therefore, the relative lack of CAOs in this winter favors the persistence of above average T_{2m}. Several blocking episodes around days 34, 61 and 71 are associated with notable peaks of T_{2m} and E_S. Animations S1-3 in the supplementary material show daily synoptic plots for each of the discussed case studies and further illustrate the interplay of the synoptic systems and the occurrence of the anomalies in the considered surface parameters.

This season's large anomaly magnitude in sub-regions **KBI** and **KBM** was mainly determined by its exceptionally positive $\overline{T_{2m}{}^*}$ and the resulting positive $\overline{H_S{}^*}$, favored by unusually frequent blocking events and the reduced frequency of CAOs throughout the season.

5.2 DJF 2016/17

The winter 2016/17 is classified as extreme in all sub-regions of the ~~Kara-Barents~~ Kara and Barents Seas. The PCA biplot shows that in **KBI** and **KBM** the anomaly magnitude of this winter is mainly determined by negative surface flux anomalies, especially of H_S (Fig. 7a and b). In **KBS**, a positive $\overline{P^*}$ is the strongest contributor to the anomaly magnitude (Fig. 7c) and in **KBM** this winter occurs with a strong positive $\overline{P^*}$ outlier (Fig. 5h). In fact, it is the winter with the most precipitation in the ~~Kara-Barents~~ Kara and Barents Seas during the study period. Further, in **KBI** and **KBM**, a strongly negative $\overline{E_S{}^*}$ occurs as a clear outlier with respect to other winters (Fig. 5j and l). Finally, $\overline{T_{2m}{}^*}$ shows a positive anomaly in **KBM** and **KBS**, which, however, is not exceptional (Fig. 5d).

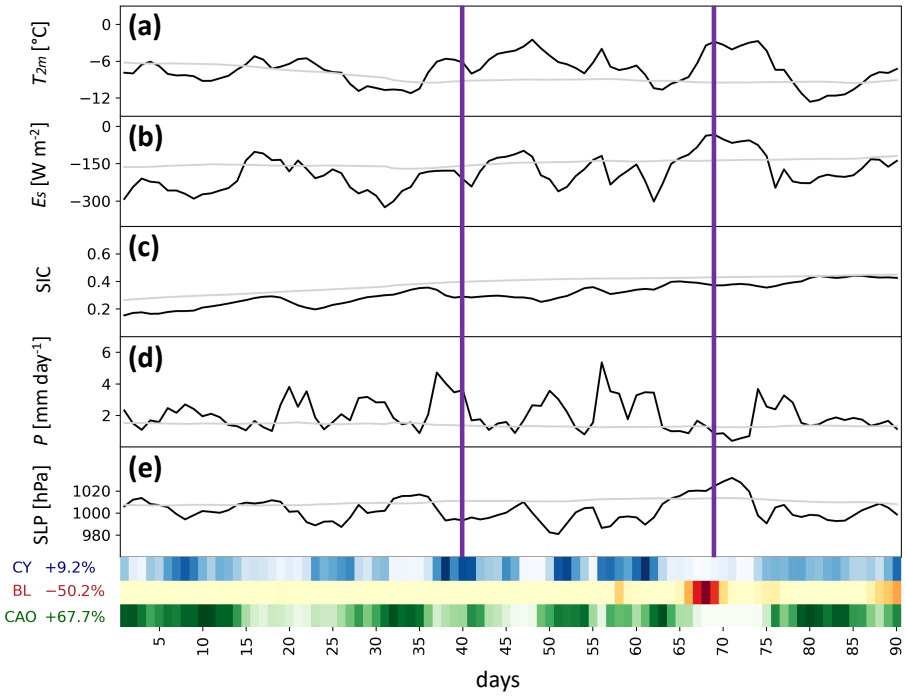

Figure 10. Time series of daily-mean **(a)** T_{2m} (in °C), **(b)** E_S (in W m^{-2}), **(c)** SIC~~and~~ , **(d)** P (in mm day^{-1}) and **(e)** sea-level pressure (SLP, in hPa) averaged in the region of the ~~Kara-Barents~~ Kara and Barents Seas (**KBI**, **KBM**, and **KBS**) in DJF 2016/17 (black lines). The transient climatology is shown by grey lines. Purple vertical lines indicate the two time steps shown in Fig. 11, 09 January 2017 (day 40) and 07 February 2017 (day 69), respectively. Blue, orange, and green heatmaps at the bottom of the figure show the daily-mean coverage of the region by cyclones, blocks, and CAOs, respectively (the darker the color the higher the coverage). Relative frequency anomalies of the three weather systems are given in percentages. The horizontal axis indicates days since the start of the season with day 1 corresponding to 01 December.

Several ~~episodic~~ precipitation events result in the strongly positive $\overline{P^*}$ which often can be linked to the passage of a cyclone (Fig. 10d, blue heatmap). Only very few episodes show P^* values below climatology, e.g. at the beginning of February when the occurrence of a block causes dry conditions (Fig. 10d, red heatmap). The positive $\overline{T_{2m}{}^*}$ results from several episodic warm events with a duration of $\sim$5–10 days (Fig. 10a), each deviating more than +5 K from climatology. There are, however, also several periods that are notably colder than climatology, thus implying a small seasonal-mean anomaly. ~~This~~ These periods typically are characterized by a CAO (Fig. 10, green heatmap). A negative SIC anomaly occurs throughout the season (Fig. 10b), which is especially pronounced in **KBM** (not shown), with strong decreases in SIC following warm and wet episodes linked to the passage of cyclones (Fig. 10, blue heatmap). During these episodes, which occur for example around days 21, 37 and 57, the wind field associated with the cyclone affects the sea ice transport and pushes the sea ice edge further north, momentarily reducing the sea ice coverage mainly in the region **KBM**. In the supplementary Fig. ~~S4~~ S7 we show an example, using

PIOMAS sea ice data (Schweiger et al., 2011), of how the passage of several cyclones between days 17 ~~December~~ and 24 ~~December~~ affects the sea ice transport in the ~~Kara-Barents~~ Kara and Barents Seas. The most prominent anomaly during this winter however is the strongly negative $\overline{E_S{}^*}$ (Fig. 10b), particularly pronounced in **KBI** and **KBM**, mainly resulting from negative $\overline{H_L{}^*}$ and $\overline{H_S{}^*}$. This negative E_S anomaly is closely linked to SIC anomalies and episodic cold periods. Specifically, the reduction in sea ice coverage and, thus, increased area of open ocean leads to more intense upward surface heat fluxes. A slightly positive tendency of E_S is found for episodes where SIC returns to climatological values, for example in February 2017 (Fig. 10b and c). In addition, the most negative values of E_S occur during cold periods related to marine CAOs (Fig. 10a and b).

Analysing the weather systems during this winter reveals that the ~~single~~ individual warm events are driven by different synoptic processes. Figure 11 ~~exemplarily shows~~ exemplifies two characteristic but different synoptic circulation patterns associated with anomalously warm conditions ~~on 09~~ in January 2017 (Fig. 11a) and ~~on 07~~ in February 2017 (Fig. 11b). In January~~2017~~, a sequence of multiple cyclones continuously transport warm air from the southwest towards the ~~Kara-Barents~~ Kara and Barents Seas (Figs. 10, blue heat map, 11a and supplementary animation S2). Figure 11a shows a typical situation where a cyclone from the Nordic Seas propagated into the ~~Kara-Barents~~ Kara and Barents Seas region, leading to anomalously warm conditions in its warm sector and precipitation along its cold front. Since the cyclones become nearly stationary and a large part of their cold sector is often located outside of the region in the Greenland Sea or towards the High Arctic, they cause a net warming in the region of the ~~Kara-Barents~~ Kara and Barents Seas as well as persistent precipitation during their passage (Fig. 10a and d). Figure 11b shows the persistent large-scale situation during the warming episode in February 2017, when a stationary block over northern Scandinavia in combination with a strong cyclone to the South of Greenland leads to anomalously warm conditions in its northern periphery (Figs. 10, red heatmap, 11b and supplementary animation S2). Next to the enhanced poleward transport of mid-latitude air masses which is favored by this pattern, subsidence-induced adiabatic warming additionally causes high surface temperatures for the duration of the block (cf. Papritz, 2020). At the same time, the presence of the block suppresses precipitation in the region, resulting in one of the driest periods of the season (Fig. 10d). In supplementary Fig. S8, we show the differences in the air mass origin for both warm events by using air parcel trajectories.

In January, daily-mean E_S values correlate well with daily-mean T_{2m} values with the most negative E_S values on the colder days. Despite ~~of~~ this, E_S shows a negative seasonal-mean anomaly, as SIC* values are strongly negative and frequent CAO events (Fig. 10, green heatmap) enhance surface fluxes into the atmosphere. In February, when SIC levels show only small negative anomalies and thus anomalous heat fluxes into the atmosphere are smaller, strong positive $H_S{}^*$, $H_L{}^*$ and $R_L{}^*$ during the blocking event lead to the largest positive $E_S{}^*$ values throughout the winter, followed again by a period with frequent CAOs and strongly negative $E_S{}^*$ values.

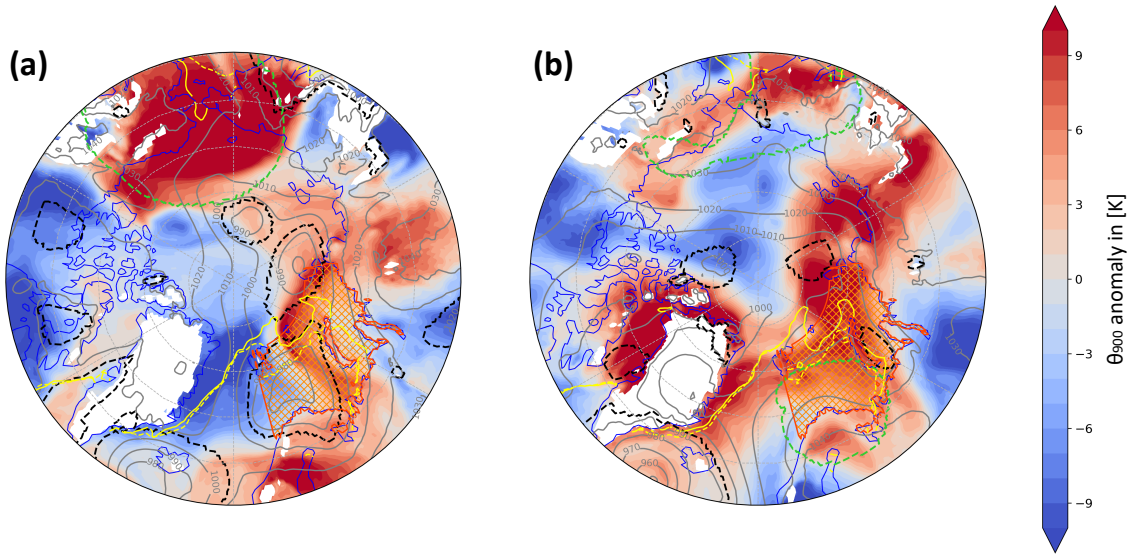

Figure 11. Synoptic situation on **(a)** 09 January 2017 (day 40) and **(b)** 07 February ~~2017.~~ 2017 (day 69). Daily anomaly of potential temperature at 900 hPa (θ_{900}; K, color). ~~Instantaneous sea-level~~ Sea-level pressure (SLP, grey ~~contour~~contours, in intervals of 10 hPa), sea ice edge (SIC = 0.5, solid yellow line), climatological sea ice edge (SIC_{clim} = 0.5, dashed yellow line), cyclone mask (dashed black contour) and blocking mask (dashed green contour) at 00 UTC on the considered days. The region of the ~~Kara-Barents~~ Kara and Barents Seas is marked by orange hatching.

Besides synoptic processes, also preconditioning potentially plays an important role for the occurrence of an extreme season, as we aim to discuss now. From Fig. 10c, it ~~is obvious~~ can be seen that SIC in the ~~Kara-Barents~~ Kara and Barents Seas was already exceptionally low at the start of the winter season, in fact, the sea ice extent on 01 December was the lowest ~~at~~ on this date for the entire study period. At the same time, the sea surface temperature (SST) shows a significantly positive anomaly of about + 1 K on average, which favors a delayed freeze-up in the region and at the same time also more intense upward sensible and latent heat fluxes. These initial surface conditions provide an important precondition for the strongly negative $\overline{E_S}^*$, which itself is decisive for the anomaly magnitude of this winter. Analysing SIC and SST anomalies in the ~~Kara-Barents~~ Kara and Barents Seas during the previous seasons in 2016 shows that they developed since the previous winter (SIC) or spring 2016 (SST, see Fig. 13b, which will be discussed in section 5.3). At the end of 2015, an extreme warm event ~~(e.g. Boisvert et al., 2016; Binder et al., 2017)~~ (e.g., Boisvert et al., 2016; Binder et al., 2017) led to a significant thinning of the sea ice in the ~~Kara-Barents~~ Kara and Barents Seas, causing an early start of the melt season in 2016 and subsequently increased SST values in MAM, coinciding with a positive $\overline{T_{2m}}^*$ in the same region. The summer of 2016 does occur as an extreme season in sub-regions **KBM** and **NOM** (Fig. 8b and e) and as an anomalous season in **KBS** (Fig. 8c), mainly due to a strong $\overline{T_{2m}}^*$ of on average + 1.4 K in the ~~Kara-Barents~~ Kara and Barents Seas, which was facilitated by a reduction

in total cloud cover and thus strongly enhanced R_S. Together with the already existing positive SST anomaly this extremely warm summer led to record low SIC and ice-free conditions in the Barents Sea from July to September (Petty et al., 2018). Strong blocking over large parts of the Arctic during ~~autumn~~ October and November 2016 caused positive surface temperature anomalies across the whole Arctic region (Tyrlis et al., 2019) as well as strong positive E_S anomalies, favoring the persistence of the negative SIC and positive SST anomalies (Blunden and Arndt, 2017) until the beginning of DJF 2016/17.

In summary, the winter 2016/17 was extreme in the Kara and Barents Seas due to a combination of preconditioning and favourable synoptic conditions. Specifically, a combination of strongly positive $\overline{\mathrm{SST}^*}$ and negative $\overline{\mathrm{SIC}^*}$ at the beginning of the season, and a relatively large number of CAO events throughout the season, resulted in strongly negative surface heat flux anomalies. Furthermore, an enhanced frequency of cyclones transporting warm and humid air masses into the region lead to a strongly enhanced $\overline{P^*}$.

5.3 Comparison of DJF 2011/12 and DJF 2016/17

Comparing both anomalous winters in the ~~Kara-Barents~~ Kara and Barents Seas, it becomes already evident from the PCA biplots (Fig. 7a and b) that the processes leading to their respective anomaly magnitude are fundamentally different, as the vectors pointing to the two seasons in the biplot are nearly orthogonal. The winter of 2011/12 is dominated by a continuous positive T_{2m} anomaly favored by a reduced frequency of CAO events, whereas in DJF 2016/17 the negative heat flux anomalies and exceptionally positive $\overline{P^*}$, enhanced by strongly reduced sea ice cover are most important. We have further seen in the previous paragraphs that both seasons feature large variability in the substructure of the respective parameters. To better understand the underlying processes leading to these differences, we will now analyse the synoptic situation in both seasons in more detail.

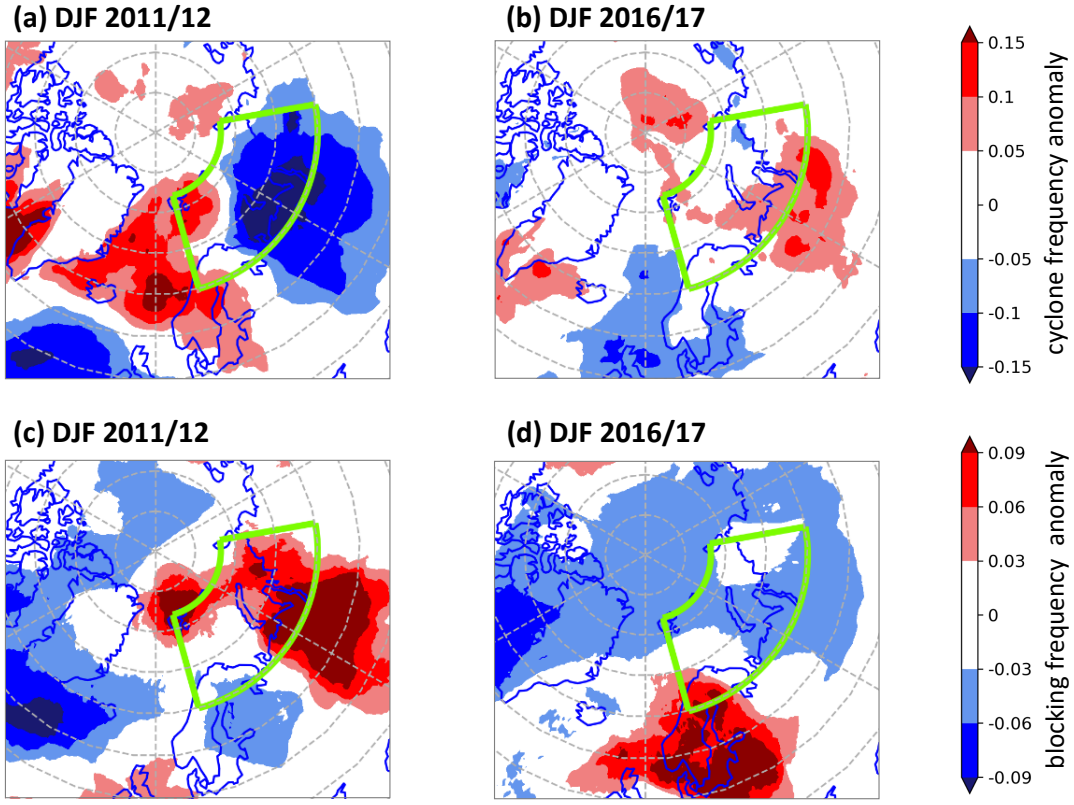

Figure 12. Seasonal-mean **(a, b)** cyclone frequency ~~**(a, b)**~~ and **(c, d)** blocking frequency ~~**(c, d)**~~ anomalies for **(a, c)** DJF 2011/12 ~~**(a, c)**~~ and **(b, d)** DJF 2016/~~17 **(b, d).** 17.~~ Region of the ~~Kara-Barents~~ Kara and Barents Seas is marked with green contour.

The synoptic activity differs between these seasons. In DJF 2011/12, cyclone frequency was strongly enhanced over the Nordic Seas concomitant with a reduction in the ~~Kara-Barents~~ Kara and eastern Barents Seas (Fig. 12a)~~. This~~ , which favored the frequent advection of warm air masses into the Barents Sea. ~~Since enhanced~~ Enhanced cyclone activity was restricted to the Nordic Seas and the western Barents Sea where several cyclones slowed down and ~~got~~ became stationary (see supplementary animation S1)~~, also the~~ . As a result, during several days of this winter, the warm sector of a cyclone was located in the Barents Seas, causing an increase in surface temperatures, whereas its cold sector was positioned in the Nordic Seas. Thus, the frequency of cold air outbreaks, which preferentially occur in the cyclone's cold sectors, was reduced in the ~~Kara-Barents Seas~~region of the Kara and Barents Seas, favoring the formation of a positive $T_{2m}{}^{*}$. In addition, recurrent blocks over the Ural mountains (Fig. 12c) contributed to above ~~normal~~ average surface temperatures. In DJF 2016/17, in contrast, cyclone activity was close to climatology (Fig. 12b) as cyclones crossed the region (see supplementary animation S2), but instead blocking frequency over Scandinavia was strongly enhanced (Fig. 12d). Subsidence-induced warming and long-range transport of warm

air masses contributed to several warm episodes ~~.~~ (see Fig. S8 in the supplement). However, an enhanced frequency of CAOs, facilitated by the frequent passage of cyclones combined with reduced SIC and warm ocean temperatures, limited $\overline{T_{2m}}^*$ but contributed to a strongly negative $\overline{E_S}^*$. Thus, the patterns of synoptic activity were partly reversed between the two seasons, yet they contributed substantially to their anomalous nature. Further, it becomes evident that the impact of cyclones on surface anomalies depends critically on their track relative to the region of interest.

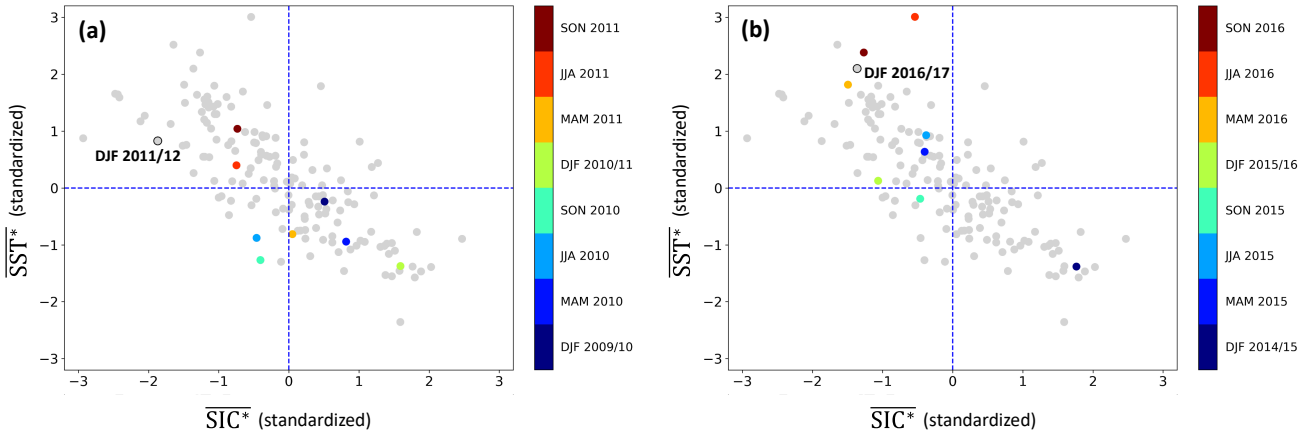

Figure 13. Standardized seasonal-mean anomalies of SIC ($\overline{\text{SIC}}^*$; along x-axis) and SST ($\overline{\text{SST}}^*$; in K, along y-axis) in the ~~Kara-Barents~~ Kara and Barents Seas for the entire study period (grey dots) including all seasons. Colored dots highlight the eight seasons preceding **(a)** the anomalous winter 2011/12 and **(b)** the extreme winter 2016/17.

In addition to the synoptic activity, we found the influence of preconditioning in SIC and SST values to be of great importance for DJF 2016/17. Figure 13b shows persistent negative $\overline{\text{SIC}}^*$ and positive $\overline{\text{SST}}^*$ throughout the preceding 1.5 years. Comparing the initial conditions for the winter of 2011/12, the influence of the previous seasons seems to be minor, as SIC and SST values are close to normal at the beginning of the winter and seasonal-mean anomalies in spring and summer 2011 show no significant negative and positive anomalies, respectively (Fig. 13a).

5.4 DJF 2012/13

After analysing two anomalous winters in the Kara and Barents Seas, we now want to discuss another anomalous Arctic winter in the High Arctic to better understand the different processes leading to such seasons in Arctic regions with distinct surface conditions. In the region of the High Arctic, the winter of 2012/13 is classified as strongly anomalous in **ARI** mainly due to its negative $\overline{T_{2m}}^*$ and $\overline{P}^*$ (Fig. 7g), making it one of the coldest and driest winters in this sub-region (Fig. 5a and e). A negative $\overline{R_L}^*$, i.e., less net longwave radiation, resulting in an overall strongly negative $\overline{E_S}^*$ contributes additionally to the anomaly magnitude of this winter (Fig. 5i). Figure 14a shows that the T_{2m} anomaly mainly results from deviations up to -8 K from

the climatology during the second half of the season, which is quite a substantial anomaly considering the size of the spatially averaged area, whereas the first half of the season is close to climatology. From mid-January on, E_S values are also consistently below average and little to no precipitation occurs until the end of the winter (Fig. 14b and e). It is evident that only the second half of the season features exceptional conditions, indicating that anomalies do not have to persist throughout a whole season to make it anomalous.

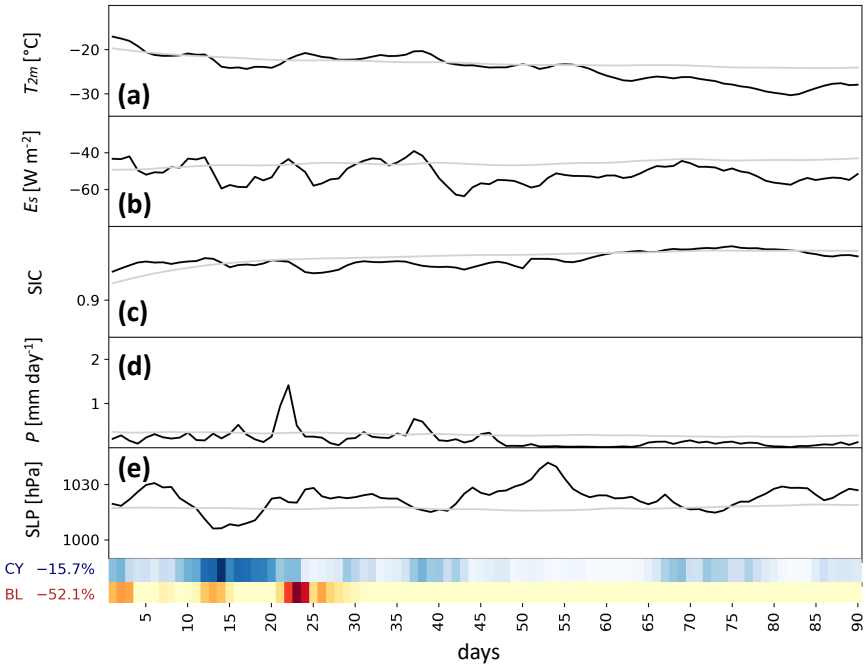

Figure 14. Time series of daily-mean **(a)** T_{2m} (in °C), **(b)** E_S (in W m^{-2}), **(c)** SIC~~and~~ , **(d)** P (in mm day^{-1}) and **(e)** sea-level pressure (SLP, in hPa) averaged in the sub-region **ARI** in DJF 2012/13 (black lines). The transient climatology is shown by grey lines. ~~Purple vertical line indicates the time step shown in Fig. ??, 18 February 2013.~~ Blue ~~, orange,~~ and ~~green~~ orange heatmaps at the bottom of the figure show the daily-mean coverage of the region by cyclones ~~,~~ and blocks, ~~and CAOs,~~ respectively (the darker the color the higher the coverage). Relative frequency anomalies of the ~~three~~ two weather systems are given in percentages. The horizontal axis indicates days since the start of the season with day 1 corresponding to 01 December.

The anomalies during the second half of the season coincide with a decrease of synoptic activity over the High Arctic. Specifically, the relative cyclone and blocking frequency anomalies in **ARI** are slightly and strongly reduced, respectively, especially in the second half of the season. In December, several cyclones and blocks affect the prevalent conditions in the High Arctic (Fig. 14, blue and red heatmaps and supplementary animation S3). Between days 20 ~~December~~ and 25~~December~~, a strong intrusion of warm and moist air facilitated by adjacent blocking and cyclone systems in the Bering Sea causes a strong

precipitation event, coinciding with increasing surface mean temperatures and a local decline in sea ice coverage (Fig. 14a, c, d). At the same time, a displacement of the polar vortex occurs, which subsequently leads to a splitting of the polar vortex and a sudden stratospheric warming event at the beginning of January 2013 (Coy and Pawson, 2015; Nath et al., 2016). As the region of the High Arctic is positioned beneath the saddle point of the resulting two cyclonic vortices in the stratosphere, relatively calm conditions lead to the development of a ~~high pressure~~ high-pressure system in the Laptev Sea, which evolves into a strong and persistent polar high during January (Fig. 14e). ~~Persistent radiative cooling induces~~ Figure 15 shows that there is no upper-level anticyclone or block present in the High Arctic during that period. This suggests that the strong high-pressure system at the surface is most likely of a thermodynamic origin caused by cold and dense air below an inversion layer (as can be seen in the skew*T*-log*p* diagram in Fig. 16), resulting from persistent radiative cooling and inducing a first drop in ~~T_{2m}~~ $T_{2m}{}^*$ at the end of January (Fig. 14a).

In February, the calm conditions in the High Arctic remain and prolong the isolation of the cold and dry air in this region. Again, a lack of notable upper-level forcing can be observed (see supplementary Fig. S9). With the increasing dryness of the air, persistent longwave radiative cooling of the surface results in a dome of very cold air, ~~as reflected by the air mass below the 275 K isentrope, covering nearly the whole High Arctic region between 17 February and 21 February (Fig. ?? and supplementary animation S3). The conditions in February cause~~ causing the formation of another surface high-pressure system during the second half of February and one of the strongest negative monthly T_{2m} anomalies in this region. The formation of the dome of cold air is evident as a strong inversion in the skew*T*-log*p* diagram (Fig. S10).

Comparing winter 2012/13 in **ARI** with the two anomalous winters in the ~~Kara-Barents~~ Kara and Barents Seas reveals fundamentally different characteristics, resulting mainly from the regionally varying synoptic activity but also the prevalent surface conditions. While preconditioning does not play an important role in the High Arctic, which is mainly covered by sea ice, the long-term development of SIC and SST anomalies in areas with varying SIC can significantly influence the initial conditions of winters in the ~~Kara-Barents~~ Kara and Barents Seas. Each of the three seasons has its own substructure and different combination of anomalies resulting in the respective anomaly magnitude. Besides the rather straightforward "continuous anomaly in one parameter" as ~~it~~ is the case for DJF 2011/12, we show that, with our approach to define extreme and anomalous seasons based on a multi-variate anomaly magnitude, there are many different pathways for such a season to develop. In DJF 2012/13, several weeks of consistent extreme conditions resulted in a whole anomalous season, although the first half of the winter was relatively normal. And in 2016/17, it was not only extraordinary atmospheric conditions but also the preconditioning by an anomalous evolution of the surface conditions during the previous months that led to an extreme Arctic winter.

6 Discussion and conclusions

In this study, Arctic winters (DJF) and summers (JJA) have been characterized based on seasonal anomalies of surface parameters including temperature, radiation, heat fluxes and precipitation for distinct regions considering varying surface conditions. In winter, strong spatial differences can be observed dependent on the prevailing surface conditions (i.e., open ocean vs. sea ice), especially in terms of the surface energy balance components (E_S), whereas in summer there is less spatial variability

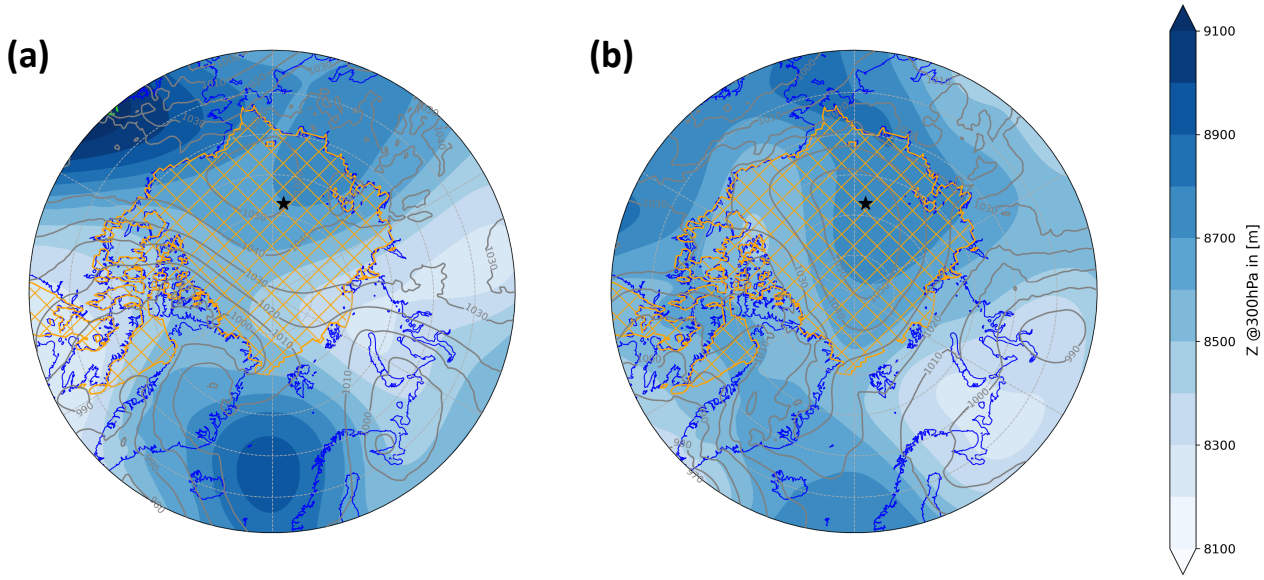

Figure 15. Synoptic situation on ~~18 February 2013.~~ **(a)** 20 January 2013 (day 51) and **(b)** 24 January 2013 (day 55). Daily ~~anomaly of the cold air mass DP, defined as the mass below the 275~~mean geopotential height at 300 ~~K isentropic surface~~ hPa (in ~~hPa~~m, color). ~~Instantaneous sea-level~~ Sea level pressure (~~SLP,~~ grey ~~contour~~contours, in intervals of 10 hPa) ~~, sea ice edge (SIC = 0.5, solid yellow line), climatological sea ice edge (SIC_{clim} = 0.5, dashed yellow line), cyclone mask (dashed black contour)~~ and blocking mask (dashed green contour) at 00 UTC on the considered days. Black star at 173 °E, 78.5 °N shows location of skew*T*-log*p* profile in Fig. 16. Sub-region **ARI** is marked by orange hatching.

595 due to reduced surface temperature and radiation gradients. Regions with a climatological sea ice concentration of above 90% show only small E_S variability mainly determined by changes in the net surface thermal radiation, as solar radiation and air-sea interactions are strongly reduced, particularly in the high latitudes. In contrast, areas with predominantly open water surface show a large seasonal variability in the surface energy balance primarily driven by fluctuations in the surface heat fluxes. Temperature anomalies do show a distinct spatial variability as well, featuring relatively large fluctuations in sea ice covered areas
600 in the Kara-Barents and Nordic Seas and reduced variability over the open ocean. The Nordic Seas are further characterized by an increased precipitation variability compared to the ~~Kara-Barents~~ Kara and Barents Seas and the High Arctic, whereby the latter shows smaller variability for all analyzed parameters.

~~Reduced surface radiation and temperature gradients as well as decreasing sea ice extent result in less heterogeneous~~
605 ~~conditions in the distinct sub-regions during summer. Only in the High Arctic, including areas of perennial sea ice, variability is clearly smaller compared to the other regions. As a consequence, the Arctic shows much more spatial variability during winter when meridional gradients in surface temperature and surface radiation are increased, leading to less homogeneous surface conditions and significant regional variability differences. Hence, it is reasonable to subdivide the Arctic into several regions~~

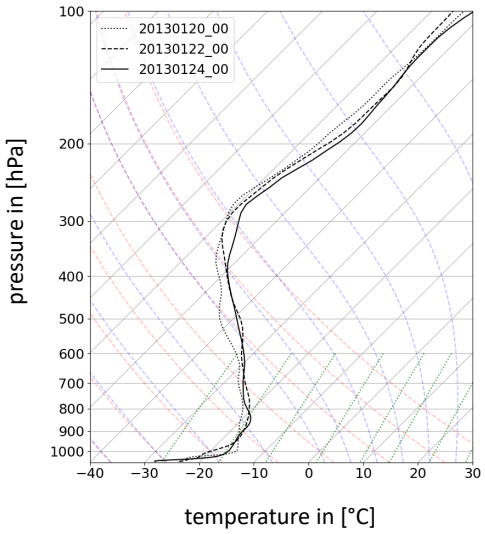

Figure 16. Skew*T*-log*p* diagram at 173 °E, 78.5 °N (black star in Fig. 15). Temperature is shown along the x-axis (in °C) and pressure along the y-axis (in hPa). Black lines show the ambient temperature profile for 20 January 2013 (day 51; dotted line), 22 January 2013 (day 53; dashed line), and 24 January 2013 (day 55; solid line) at 00 UTC. Grey lines show isobars (horizontal) and isotherms (skewed), respectively. Colored dashed lines denote dry (red) and moist (blue) adiabats, respectively. Green dotted lines denote constant saturation mixing ratios.

~~considering these spatial differences to study anomalous Arctic winter seasons.~~ We further characterized Arctic seasons based on the seasonal substructure of surface temperature (T_{2m}), precipitation (P) and E_S. Continuous seasonal anomalies, indicating constantly anomalous conditions of the same sign throughout a whole season, can be observed for T_{2m} and E_S except for the open ocean, where strong surface heat flux variability prevents continuous E_S anomalies. Distinct outlier seasons can be observed featuring exceptional seasonal-mean anomalies in one or several parameter(s).

To define and identify anomalous and extreme seasons objectively, we introduce a ~~novel,~~ multi-variate method. Using PCA, we define anomalous and extreme seasons by means of an anomaly magnitude based on the combination of seasonal anomalies of T_{2m}, P, surface heat fluxes and surface net radiation. ~~This~~ Unlike conventional, univariate approaches, we do not pre-define and thus prioritize one particular parameter by simply choosing, e.g., the warmest or wettest seasons. Instead, our multi-variate approach has the advantage ~~over a univariate approach~~ that it also allows to identify seasons that arise from an unusual combination of seasonal anomalies that taken alone are not particularly unusual. ~~We~~ This consequently leads to different types of extreme seasons in terms of their individual anomalies which, however, share a similar "unusualness" as expressed by the anomaly magnitude d_M. In order to reach a significant d_M value, at least one of the considered variables or a combination thereof must be clearly exceptional compared to other seasons. We can show that all of our extreme seasons have very large anomalies for at least one parameter and thus would most probably be found to be extreme with a more conventional approach

as well. We find that our identified anomalous seasons often result from various combinations of unusual seasonal anomalies, which allows us to analyse a broader spectrum of unusual seasons with regard to their underlying processes and atmospheric dynamics. Further, using a multivariate approach allows us to compare extreme and anomalous Arctic seasons considering the heterogeneity of the Arctic surface. We analyze sub-regions with climatologically high, mixed or low sea ice cover separately, thus accounting for regional differences in the surface conditions, which have a strong impact on the variability of these parameters. ~~With this approach, we find that our identified extreme and anomalous seasons result from various combinations of unusual seasonal anomalies.~~

Based on this definition of extreme seasons, we analyzed the atmospheric processes leading to three selected extreme and anomalous winter seasons by evaluating the relative importance of different synoptic features, namely cyclones, blocks and cold air outbreaks (CAO). This helps improving the understanding of the formation of such seasons and underlines the manifold processes that can cause a season to become particularly unusual. The results of our analysis for three different case studies can be summarized as follows:

1. Seasonal substructure: Extreme and anomalous Arctic winter seasons show a high variability in their substructure and the synoptic processes determining their anomaly magnitude. This magnitude can be due to a continuous seasonal anomaly in one parameter such as it is the case for the constantly positive temperature anomaly during the exceptionally warm winter 2011/12 in the ~~Kara-Barents~~ Kara and Barents Seas. However, also the combination of several noticeable but not exceptional seasonal anomalies can result in a similarly large anomaly magnitude. Furthermore, extreme conditions do not need to persist during a whole season as we can see for the winter of 2012/13 in the High Arctic, where several weeks of persistent cold and dry conditions caused seasonal anomalies that are sufficiently large for the season to be identified as anomalous.

2. Atmospheric processes: Various synoptic processes can cause Arctic winters to become anomalous or extreme. An increase in cyclone frequency often leads to enhanced transport of warm and moist air into the respective region, which is particularly important for the formation of precipitation in the higher latitudes. Episodes of prevailing atmospheric blocking usually favor the persistence of positive surface temperature anomalies due to subsidence-induced adiabatic warming. Recurrent synoptic events such as cyclones, blocking and CAO episodes can strongly influence the entire season, depending on their location relative to the considered region. Similarly, the absence of synoptic activity can be important for the development of extreme conditions as can be seen in the case of the High Arctic extreme winter 2012/13. Contrasting synoptic conditions can lead to extreme seasons in the ~~Kara-Barents~~ Kara and Barents Seas, which, however, show very different characteristics. Further, the frequency of CAOs strongly influences surface temperature anomalies and changes in E_S mainly due to the impact on air-sea interaction.

3. Surface preconditioning: Regions with varying sea ice coverage can experience preconditioning due to long-term anomalies in sea ice concentration (SIC) and sea surface temperature (SST), leading to anomalous initial conditions at the beginning of the season and thus influencing the sea ice formation and E_S throughout the following winter. Large SIC

and SST anomalies, which developed and persisted throughout the preceding 1.5 years, led to record-low SIC and above average SST in the ~~Kara-Barents~~ Kara and Barents Seas at the beginning of the winter of 2016/17. Due to the increased amount of open water area, predominantly negative surface heat flux anomalies prevailed throughout the season, resulting in an exceptionally negative seasonal E_S anomaly. This suggests that extreme and anomalous seasons in regions with a climatological sea ice concentration between 10 % and 90 % can be caused by such a preconditioning, whereas extreme and anomalous seasons in regions with continuous sea ice extent are mainly driven by atmospheric processes.

One of the main limitations of this study is the short time-period for which the ERA5 data is currently available. As our goal is to study anomalous seasons, the number of suitable cases is strongly limited. Future analysis of large ensemble simulations of the CESM climate model will allow us to further statistically quantify and confirm the results of this study. The importance of long-term components such as the near-surface ocean processes leading to possible preconditioning of anomalous seasons have only been briefly considered in this study. Further analysis of anomalies in surface oceanic heat transport and its influence on sea ice formation and melt and sea surface temperatures will allow us to quantify the relative importance of short-term atmospheric and long-term oceanic forcing in driving the processes leading to Arctic extreme seasons.

Code and data availability. ERA5 data can be downloaded from the Copernicus Climate Data Store (https://cds.climate.copernicus.eu/). The PIOMAS data set can be obtained from the Polar Science Center web page (http://psc.apl.uw.edu/research/projects/arctic-sea-ice-volume-anomaly/data/). Scripts used to produce the analyses and figures in this study are available on request from the authors.

Author contributions. KH performed most of the analyses, produced all figures and wrote the initial draft of the manuscript. All authors contributed to the design of the study, the understanding and interpretation of the results and the writing of the paper.

Competing interests. The authors declare that they have no competing interests.

Acknowledgements. KH and MB acknowledge funding by the European Research Council 485 (ERC) under the European Union's Horizon 2020 research and innovation programme (project INTEXseas, grant agreement no. 787652). We thank Mauro Hermann and Matthias Röthlisberger for input and helpful discussions, and Michael Sprenger (all ETH Zurich) for his help with preparing the ERA5 data. KH thanks Katharina Heitmann for feedback on the first draft of the manuscript. The authors acknowledge MeteoSwiss and ECWMF for providing access to the ERA5 reanalyses. We thank Irina Rudeva, two anonymous reviewers, and the Editor Camille Li for their constructive feedback that helped to clarify and strengthen the presentation of our results.

References

Arrhenius, S.: On the influence of carbonic acid in the air upon the temperature of the ground, Philos. Mag. J. Sci., 5, 237–276, https://doi.org/https://doi.org/10.1080/14786449608620846, 1896.

Binder, H., Boettcher, M., Grams, C. M., Joos, H., Pfahl, S., and Wernli, H.: Exceptional air mass transport and dynamical drivers of an extreme wintertime Arctic warm event, Geophys. Res. Lett., 44, 12 028–12 036, https://doi.org/10.1002/2017GL075841, 2017.

Blunden, J. and Arndt, D. S.: State of the Climate in 2016, Bull. Amer. Meteor. Soc., 98, Si–S277, https://doi.org/10.1175/2017BAMSStateoftheClimate.1, 2017.

Boisvert, L. N., Petty, A. A., and Stroeve, J. C.: The impact of the extreme winter 2015/16 Arctic cyclone on the Barents–Kara Seas, Mon. Wea. Rev., 144, 4279–4287, https://doi.org/10.1175/MWR-D-16-0234.1, 2016.

Cavalieri, D. J. and Parkinson, C. L.: Arctic sea ice variability and trends, 1979-2010, https://doi.org/10.5194/tc-6-881-2012, 2012.

Cohen, J., Screen, J. A., Furtado, J. C., Barlow, M., Whittleston, D., Coumou, D., Francis, J., Dethloff, K., Entekhabi, D., Overland, J., and Jones, J.: Recent Arctic amplification and extreme mid-latitude weather, Nat. Geosci., 7, 627–637, https://doi.org/10.1038/ngeo2234, 2014.

Coy, L. and Pawson, S.: The major Stratospheric Sudden Warming of January 2013: Analyses and forecasts in the GEOS-5 data assimilation system, Mon. Wea. Rev., 143, 491–510, https://doi.org/10.1175/MWR-D-14-00023.1, 2015.

Croci-Maspoli, M., Schwierz, C., and Davies, H. C.: A multifaceted climatology of atmospheric blocking and its recent linear trend, J. Clim., 20, 633–649, 2007.

Cullather, R. I., Lim, Y.-K., Boisvert, L. N., Brucker, L., Lee, J. N., and Nowicki, S. M. J.: Analysis of the warmest Arctic winter, 2015-2016, Geophys. Res. Lett., 43, 10 808–10 816, https://doi.org/10.1002/2016GL071228, 2016.

Curry, J. A., Schramm, J. L., and Ebert, E. E.: Sea ice-albedo climate feedback mechanism, J. Clim., 8, 240–247, https://doi.org/10.1175/1520-0442(1995)008<0240:SIACFM>2.0.CO;2, 1995.

Dickson, R., Lazier, J., Meincke, J., Rhines, P., and Swift, J.: Long-term coordinated changes in the convective activity of the North Atlantic, Prog. Oceanogr., 38, 241–295, https://doi.org/10.1016/S0079-6611(97)00002-5, 1996.

Ding, Q., Schweiger, A., L'Heureux, M., Battisti, D., Po-Chedley, S., Johnson, N., Blanchard-Wrigglesworth, E., Harnos, K., Zhang, Q., Eastman, R., and Steig, E.: Influence of high-latitude atmospheric circulation changes on summertime Arctic sea ice, Nat. Clim. Change, 7, 289–295, https://doi.org/10.1038/nclimate3241, 2017.

Gabriel, K. R.: The biplot graphic display of matrices with application to principal component analysis, Biometrika, 58, 453–467, https://doi.org/https://doi.org/10.2307/2334381, 1971.

Gabriel, K. R.: Analysis of Meteorological Data by Means of Canonical Decomposition, J. Appl. Meteorol., 11, 1071–1077, https://doi.org/https://doi.org/10.1175/1520-0450(1972)011<1071:AOMDBM>2.0.CO;2, 1972.

Graf, M. A., Wernli, H., and Sprenger, M.: Objective classification of extratropical cyclogenesis, Q. J. Roy. Meteor. Soc., 143, 1047–1061, https://doi.org/10.1002/qj.2989, 2017.

Graversen, R. G. and Burtu, M.: Arctic amplification enhanced by latent energy transport of atmospheric planetary waves, Q. J. Roy. Meteor. Soc., 142, 2046–2054, https://doi.org/10.1002/qj.2802, 2016.

Graversen, R. G. and Wang, M.: Polar amplification in a coupled climate model with locked albedo, Climate Dyn., 33, 629–643, https://doi.org/10.1007/s00382-009-0535-6, 2009.

Harden, B. E., Renfrew, I. A., and Petersen, G. N.: Meteorological buoy observations from the central Iceland Sea, Geophys. Res. Atmos., 120, 3199–3208, https://doi.org/10.1002/2014JD022584, 2015.

Hermann, M., Papritz, L., and Wernli, H.: A Lagrangian analysis of the dynamical and thermodynamic drivers of Greenland melt events during 1979-2017, Weather Clim. Dynam., 1, 497–518, https://doi.org/https://doi.org/10.5194/wcd-1-497-2020, 2020.

Hersbach, H., Bell, B., Berrisford, P., Hirahara, S., Horányi, A., Muñoz-Sabater, J., Nicolas, J., Peubey, C., Radu, R., Schepers, D., Simmons, A., Soci, C., Abdalla, S., Abellan, X., Balsamo, G., Bechtold, P., Biavati, G., Bidlot, J., Bonavita, M., De Chiara, G., Dahlgren, P., Dee, D., Diamantakis, M., Dragani, R., Flemming, J., Forbes, R., Fuentes, M., Geer, A., Haimberger, L., Healy, S., Hogan, R. J., Hólm, E., Janisková, M., Keeley, S., Laloyaux, P., Lopez, P., Lupu, C., Radnoti, G., de Rosnay, P., Rozum, I., Vamborg, F., Villaume, S., and Thépaut, J. N.: The ERA5 global reanalysis, Q. J. Roy. Meteor. Soc., 146, 1999–2049, https://doi.org/10.1002/qj.3803, 2020.

Johannessen, O. M., Kuzmina, S. I., Bobylev, L. P., and Miles, M. W.: Surface air temperature variability and trends in the Arctic: new amplification assessment and regionalisation, Tellus A, 68, 28 234, https://doi.org/10.3402/tellusa.v68.28234, 2016.

Laliberté, F. and Kushner, P. J.: Midlatitude moisture contribution to recent Arctic tropospheric summertime variability, J. Clim., 27, 5693–5707, https://doi.org/10.1175/JCLI-D-13-00721.1, 2014.

Lindsay, R. W.: Temporal variability of the energy balance of thick Arctic pack ice, J. Clim., 11, 313–333, https://doi.org/10.1175/1520-0442(1998)011<0313:TVOTEB>2.0.CO;2, 1998.

Liu, C. and Barnes, E. A.: Extreme moisture transport into the Arctic linked to Rossby wave breaking, J. Geophys. Res.: Atmos., 120, 3774–3788, https://doi.org/10.1002/2014JD022796, 2015.

Marshall, J. and Schott, F.: Open-ocean convection: Observations, theory, and models, Rev. Geophys., 37, 1–64, https://doi.org/10.1029/98RG02739, 1999.

Martius, O. and Rivière, G.: Rossby wave breaking: climatology, interaction with low-frequency climate variability, and links to extreme weather events, in: Dynamics and predictability of large-scale, high-impact weather and climate events, edited by Li, J., Swinbank, R., Grotjahn, R., and Volkert, H., pp. 69–78, Cambridge University Press, Cambridge, https://doi.org/10.1017/CBO9781107775541.006, 2016.

Messori, G., Woods, C., and Caballero, R.: On the drivers of wintertime temperature extremes in the High Arctic, J. Clim., 31, 1597–1618, https://doi.org/10.1175/JCLI-D-17-0386.s1, 2018.

Nath, D., Chen, W., Zelin, C., Pogoreltsev, A. I., and Wei, K.: Dynamics of 2013 Sudden Stratospheric Warming event and its impact on cold weather over Eurasia: Role of planetary wave reflection, Scientific Reports, 6, 24 174, https://doi.org/10.1038/srep24174, 2016.

Nghiem, S. V., Hall, D. K., Mote, T. L., Tedesco, M., Albert, M. R., Keegan, K., Shuman, C. A., DiGirolamo, N. E., and Neumann, G.: The extreme melt across the Greenland ice sheet in 2012, Geophys. Res. Lett., 39, L20 502, https://doi.org/10.1029/2012GL053611, 2012.

North, G. R., Bell, T. L., Cahalan, R. F., and Moeng, F. J.: Sampling errors in the estimation of Empirical Orthogonal Functions, Mon. Wea. Rev., 110, 699–706, 1982.

Ohmura, A.: Present status and variations in the Arctic energy balance, Polar Sci., 6, 5–13, https://doi.org/10.1016/j.polar.2012.03.003, 2012.

Olonscheck, D., Mauritsen, T., and Notz, D.: Arctic sea-ice variability is primarily driven by atmospheric temperature fluctuations, Nature Geoscience, 12, 430–434, https://doi.org/10.1038/s41561-019-0363-1, 2019.

Papritz, L.: Arctic lower-tropospheric warm and cold extremes: Horizontal and vertical transport, diabatic processes, and linkage to synoptic circulation features, J. Clim., 33, 993–1016, https://doi.org/10.1175/JCLI-D-19, 2020.

Papritz, L. and Dunn-Sigouin, E.: What configuration of the atmospheric circulation drives extreme net and total moisture transport into the Arctic, Geophys. Res. Lett., 47, e2020GL089 769, https://doi.org/10.1029/2020GL089769, 2020.

Papritz, L. and Spengler, T.: A Lagrangian climatology of wintertime cold air outbreaks in the Irminger and Nordic Seas and their role in shaping air-sea heat fluxes, J. Clim., 30, 2717–2737, https://doi.org/10.1175/JCLI-D-16-0605.1, 2017.

Petty, A. A., Stroeve, J. C., Holland, P. R., Boisvert, L. N., Bliss, A. C., Kimura, N., and Meier, W. N.: The Arctic sea ice cover of 2016: a year of record-low highs and higher-than-expected lows, The Cryosphere, 12, 433–452, https://doi.org/10.5194/tc-12-433-2018, 2018.

Pithan, F. and Mauritsen, T.: Arctic amplification dominated by temperature feedbacks in contemporary climate models, Nat. Geosci., 7, 181–184, https://doi.org/10.1038/ngeo2071, 2014.

Pithan, F., Svensson, G., Caballero, R., Chechin, D., Cronin, T. W., Ekman, A. M. L., Neggers, R., Shupe, M. D., Solomon, A., Tjernström, M., and Wendisch, M.: Role of air-mass transformations in exchange between the Arctic and mid-latitudes, Nat. Geosci., 11, 805–812, https://doi.org/10.1038/s41561-018-0234-1, 2018.

Pope, J. O., Bracegirdle, T. J., Renfrew, I. A., and Elvidge, A. D.: The impact of wintertime sea-ice anomalies on high surface heat flux events in the Iceland and Greenland Seas, Clim. Dynam., 54, 1937–1952, https://doi.org/10.1007/s00382-019-05095-3, 2020.

Röthlisberger, M., Hermann, M., Frei, C., Lehner, F., Fischer, E. M., Knutti, R., and Wernli, H.: A new framework for identifying and investigating seasonal climate extremes, J. Clim. (in press), https://doi.org/10.1175/JCLI-D-20-0953.1, 2021.

Schweiger, A., Lindsay, R., Zhang, J., Steele, M., Stern, H., and Kwok, R.: Uncertainty in modeled Arctic sea ice volume, J. Geophys. Res., 116, C00D06, https://doi.org/10.1029/2011JC007084, 2011.

Schwierz, C., Croci-Maspoli, M., and Davies, H. C.: Perspicacious indicators of atmospheric blocking, Geophys. Res. Lett., 31, L06 125, 2004.

Segtnan, O. H., Furevik, T., and Jenkins, A. D.: Heat and freshwater budgets of the Nordic Seas computed from atmospheric reanalysis and ocean observations, J. Geophys. Res., 116, C11 003, https://doi.org/10.1029/2011JC006939, 2011.

Serreze, M. C. and Barry, R. G.: Processes and impacts of Arctic amplification: A research synthesis, Glob. Planet. Change, 77, 85–96, https://doi.org/10.1016/j.gloplacha.2011.03.004, 2011.

Serreze, M. C. and Francis, J. A.: The Arctic amplification debate, Climatic Change, 76, 241–264, https://doi.org/10.1007/s10584-005-9017-y, 2006.

Simmonds, I. and Rudeva, I.: The great Arctic cyclone of August 2012, Geophys. Res. Lett., 39, L23 709, https://doi.org/10.1029/2012GL054259, 2012.

Sorteberg, A. and Walsh, J. E.: Seasonal cyclone variability at 70°N and its impact on moisture transport into the Arctic, Tellus A, 60, 570–586, https://doi.org/10.1111/j.1600-0870.2008.00314.x, 2008.

Sprenger, M., Fragkoulidis, G., Binder, H., Croci-Maspoli, M., Graf, P., Grams, C. M., Knippertz, P., Madonna, E., Schemm, S., Škerlak, B., and Wernli, H.: Global climatologies of Eulerian and Lagrangian flow features based on ERA-Interim, B. Am. Meteotol. Soc., 98, 1739–1748, https://doi.org/10.1175/BAMS-D-15-00299.1, 2017.

Stroeve, J., Frei, A., McCreight, J., and Ghatak, D.: Arctic sea-ice variability revisited, Ann. Glaciol., 48, 71–81, https://doi.org/10.3189/172756408784700699, 2008.

Talley, L. D.: Freshwater transport estimates and the global overturning circulation: Shallow, deep and throughflow components, Prog. Oceanogr., 78, 257–303, https://doi.org/10.1016/j.pocean.2008.05.001, 2008.

Tyrlis, E., Manzini, E., Bader, J., Ukita, J., Nakamura, H., and Matei, D.: Ural blocking driving extreme Arctic sea ice loss, cold Eurasia, and stratospheric vortex weakening in autumn and early winter 2016–2017, J. Geophys. Res.: Atmos., 124, 11 313–11 329, https://doi.org/10.1029/2019JD031085, 2019.

Vavrus, S.: The impact of cloud feedbacks on Arctic climate under greenhouse forcing, J. Clim., 17, 603–615, https://doi.org/10.1175/1520-0442(2004)017<0603:TIOCFO>2.0.CO;2, 2004.

Webster, M. A., Parker, C., Boisvert, L., and Kwok, R.: The role of cyclone activity in snow accumulation on Arctic sea ice, Nat. Commun., 10, 5285, https://doi.org/10.1038/s41467-019-13299-8, 2019.

Wernli, H. and Papritz, L.: Role of polar anticyclones and mid-latitude cyclones for Arctic summertime sea-ice melting, Nat. Geosci., 11, 108–113, https://doi.org/10.1038/s41561-017-0041-0, 2018.

Wernli, H. and Schwierz, C.: Surface cyclones in the ERA-40 dataset (1958–2001). Part I: Novel identification method and global climatology, J. Atmos. Sci., 63, 2486–2507, https://doi.org/10.1175/jas3766.1, 2006.

White, D., Hinzman, L., Alessa, L., Cassano, J., Chambers, M., Falkner, K., Francis, J., Gutowski, W. J., Holland, M., Holmes, R. M., Huntington, H., Kane, D., Kliskey, A., Lee, C., McClelland, J., Peterson, B., Rupp, T. S., Straneo, F., Steele, M., Woodgate, R., Yang, D., Yoshikawa, K., and Zhang, T.: The Arctic freshwater system: Changes and impacts, J. Geophys. Res., 112, G04S54, https://doi.org/10.1029/2006JG000353, 2007.

Woods, C. and Caballero, R.: The role of moist intrusions in winter Arctic warming and sea ice decline, J. Clim., 29, 4473–4485, https://doi.org/10.1175/JCLI-D-15-0773.1, 2016.

Woods, C., Caballero, R., and Svensson, G.: Large-scale circulation associated with moisture intrusions into the Arctic during winter, Geophys. Res. Lett., 40, 4717–4721, https://doi.org/10.1002/grl.50912, 2013.